Hadassa Reinskjen Leite do Valle

Bachelor in Micro and Nanotechnologies Engineering

Effect of eco-friendly solvents in solution-based ZrO_x dielectrics

Dissertation submitted in partial fulfilment
of the requirements for the degree of

Master of Science in
Micro and Nanotechnologies Engineering

Supervisor: Rita Maria Mourão Salazar Branquinho,
Assistant Professor, NOVA University
of Lisbon (FCT-UNL)

Examination committee:

Chair: Prof. Dr. Hugo Águas
Rapporteur(s): Prof. Dr. Rui Igreja
Member(s): Prof. Dr. Rita Branquinho

FACULDADE DE CIÊNCIAS E TECNOLOGIA
UNIVERSIDADE NOVA DE LISBOA

December, 2019

Effect of eco-friendly solvents in solution-based ZrO_x dielectrics

Acknowledgments

First, I would like to thank Prof. Dr. Rodrigo Martins and Prof. Dr. Elvira Fortunato for creating the course of Micro and Nanotechnology and for all their hard work and commitment to the research centers of CENIMAT| I3N and CEMOP, which provided everything I needed during my thesis.

My special acknowledge goes to my supervisor, Prof. Dr. Rita Branquinho and to the PhD student, Emanuel Carlos, for their extensive help and guidance providing meetings every month, showing the correct laboratories procedures and analysing my thesis, despite their busy schedule. It would be much harder overcome all the difficulties without them and all the words would be insufficient to thank for everything.

To all my docents, professors and researchers for all the sharing of knowledge that will be essential to my future. Thank you as well to all my colleagues and friends of Micro and Nanotechnology that accompanied me throughout the academic life to make this experience so much funnier. I will never forget our memories together.

To my fellow colleagues that accompanied me throughout the thesis, thank you for all the energy and laughs in the early morning and for helping whenever I needed.

I would also like to thank my family and closest friends who have supported me throughout this journey, for their motivation, capability of listen and for all the advices that were extremely important to make me who I am today. You are my inspiration.

To my mom, for her incredible support and for being outstandingly comprehensive even during the hard times.

To my dad, for caring about me and for always keeping in touch even with this long distance between us.

To my grandparents, uncles and brothers for all the support and love.

Abstract

Over the past decade, solution-based dielectric oxides have been widely studied in electronic applications, enabling the use of low-cost processing technologies and device improvement. Among many high-κ dielectrics, zirconium oxide (ZrO_x) has been regarded as one of the most promising inorganic dielectric materials for its excellent properties. This work aims to study the effect of environmentally friendly solvents, in order to replace the conventional ones and obtain a safer working environment and optimize solution-based ZrO_x. dielectrics. For this, ZrO_x thin films were produced with different solvents and different process conditions by sol-gel method. Its microstructure and electronic properties as dielectrics in thin films metal-insulator-semiconductor structured capacitors for high-frequency circuits were investigated systematically. It was found that the capacitors obtained from a zirconium nitrate-based precursor solution with a concentration of 0.2 M in 2-methoxyethanol (2-ME) annealed at 300 °C showed an average dielectric constant of 8.7 ± 0.6 and a low leakage current density of (2.2 ± 2.7) × 10^{-8} A/cm^2 at 1 MV/cm. However, 2-ME is a toxic solvent that can cause serious harm to human health as such eco-friendly solvents were tested. Ethanol-based ZrO_x capacitors were successfully produced at 300 °C showing an average dielectric constant of 10.8 ± 0.2 and a leakage current density of (8.7 ± 0.4) × 10^{-7} A/cm^2 at 1 MV/cm. Looking towards the future of electronics, metal-insulator-metal capacitors were processed on a flexible substrate at a low temperature of 150 °C combined with deep ultra-violet (DUV) irradiation, showing an average dielectric constant 11 ± 1 and a low leakage current density of (4.7 ± 4.7) × 10^{-7} A/cm^2 at 0.5 MV/cm. Finally, the optimized ZrO_x dielectric thin films were successfully applied as gate insulator in solution-processed In_2O_3 TFTs.

Keywords: Zirconium Oxide (ZrO_x), Eco-friendly Solvents, Low Temperature, TFTs, Solution Process, High-κ Dielectric

Resumo

Na última década, os óxidos dielétricos baseados em soluções têm sido amplamente estudados em aplicações eletrônicas, possibilitando o uso de tecnologias de processamento de baixo custo e melhoria de dispositivos. Entre muitos dielétricos de alto κ, o óxido de zircónio (ZrO_x) tem sido considerado um dos materiais dielétricos inorgânicos mais promissores por suas excelentes propriedades. Esse trabalho tem como objetivo estudar o efeito de solventes ecológicos, a fim de substituir os convencionais e obter um ambiente de trabalho mais seguro, e otimizar ZrO_x dielétricos baseados em solução. Para isso, filmes finos de ZrO_x foram produzidos com diferentes solventes e diferentes condições de processo pelo método sol-gel. As suas microestruturas e propriedades eletrônicas como dielétricos em metal-isolador-semiconductor capacitores de filmes finos para circuitos de alta frequência foram investigados sistematicamente. Verificou-se que os capacitores obtidos a partir de uma solução precursora à base de nitrato de zircónio com uma concentração de 0.2 M em 2-metoxietanol (2-ME) recozido a 300 °C apresentaram uma constante dielétrica média de 8.7 ± 0.6 e uma baixa corrente de fuga de (2.2 ± 2.7) × 10^{-8} A / cm^2 a 1 MV/cm. No entanto, o 2-ME é um solvente tóxico que pode causar sérios danos à saúde humana, sendo assim solventes ecológicos foram testados. Os ZrO_x à base de etanol foram produzidos com sucesso a 300 °C, mostrando uma constante dielétrica média de 10.8 ± 0.2 e uma densidade de corrente de fuga de (8.7 ± 0.4) × 10^{-7} A / cm^2 a 1 MV/cm. Olhando para o futuro da eletrónica, metal-isolador-metal capacitores foram processados num substrato flexível a uma temperatura baixa de 150 °C combinada com irradiação DUV, mostrando uma constante dielétrica média 11 ± 1 e uma baixa corrente de fuga de (4.7 ± 4.7) × 10^{-7} A / cm^2 a 0.5 MV/cm. Finalmente, os filmes finos dielétricos ZrO_x otimizados foram aplicados com sucesso como isoladores de porta em In_2O_3 TFTs processados por solução.

Palavras-chave: Óxido de Zircónio, Solventes Ecológicos, Baixa Temperatura, TFTs, Processamento por Solução, Dielétrico com Alto κ

List of Abbreviations

AFM	Atomic Force Microscopy
ALD	Atomic Layer Deposition
ATR	Attenuated Total Reflectance
CCM	Conventional Combustion Method
CEMOP	Center of Excellence in Microelectronics and Optoelectronics Processes
CENIMAT	Materials Research Center
C-f	Capacitance-frequency
C-V	Capacitance-Voltage
DMF	Dimethylformamide
DSC	Differential Scanning Calorimetry
DUV	Deep Ultraviolet
EHS	Environment, Health & Safety method
EOT	Equivalent Oxide Thickness
FTIR	Fourier Transform Infrared Spectroscopy
FUV	Far Ultraviolet
GIXRD	Grazing Incidence X-Ray Diffractometer
ILs	Ionic Liquids
I-V	Current-Voltage
LCA	Life-Cycle Assessment
M-O-M	Metal-Oxide-Metal
MIM	Metal-Insulator-Metal
MIS	Metal-Insulator-Semiconductor
MOS	Metal Oxide Semiconductor
MOSFET	Metal Oxide Semiconductor Field Effect Transistor

OV	Oxidizing Valence
PEN	Polyethylene Naphthalate
PET	Polyethylene Terephthalate
PTFE	Polytetrafluoroethylene
RV	Reducing Valence
SCS	Solution Combustion Synthesis
SEM	Scanning Electron Microscopy
TFTs	Thin Film Transistors
TG	Thermogravimetry
U	Urea
UV	Ultraviolet
Vis	Visible
VOSs	Volatile Organic Solvents
XRD	X-Ray Diffraction

List of Symbols

A	Area
c	Concentration
C	Capacitance
C_{i}	Capacitance per unit area
C_{D}	Capacitance of semiconductor depletion
C_{ox}	Capacitance of the oxide film
C_{s}	Capacitance of silicon surface
d	Thickness of the insulator layer
$d_{\mathrm{high-\kappa}}$	Thickness of the high-κ dielectric layer
d_{ox}	Equivalent thickness of the SiO_2 material
$\boldsymbol{E}$	Breakdown Electric Field
E_{g}	Band gap energy
ε_0	Permittivity of free space (8.885×10^{-12} F m^{-1})
f	Frequency
I_{D}	Drain Current
I_{G}	Gate leakage current
I_{ON}	Drain current in the on state
I_{OFF}	Drain current in the off state
J	Density of leakage current
κ	Dielectric constant of the insulating material
L	Channel Length
n	Number of moles
OV	Valency of the oxidizing reagent
Q	Charge
SS	Subthreshold Swing

t_A	Annealing time
μ_{sat}	Saturation mobility
V_{DS}	Voltage between drain and source
V_{FB}	Flat band voltage
V_G	Gate voltage
V_T	Threshold voltage
W	Channel Width
°C	Degrees Celsius
ϕ	Fuel/oxidizer ratio

Table of Contents

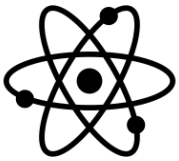

List of Figures

List of Tables

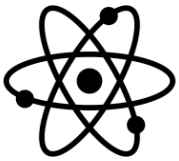

Motivation and Objectives

Recent developments in electronics have led to the availability of unprecedented products such as flat panel displays, smart phones and sensor arrays in our daily life. For the next generation of large area electronics (transparent, flexible, and wearable devices), the thin-film transistor (TFT), which is an essential basic building block for electronic devices, should exhibit additional functionalities, such as optical transparency and inexpensive cost for large area application. The current technology do not fulfil these requirements, so in order to achieve the improved performance of these devices, two tasks have to be done: a study and optimization of more appropriate gate dielectrics to substitute the conventional SiO_2, which will allow low power consumption; a study and optimization of solution-based processes, compatible with large-area being able to substitute the expensive and low-throughput vacuum-based methods, at low process temperature.

Solution-processable high-κ dielectrics have been reported as materials capable of reducing the leakage currents even when produced as ultrathin layers, the operation voltage and the power consumption of the devices. Among others, zirconium oxide (ZrO_x) films have been applied as dielectric in capacitors and gate insulator in TFTs for some researches groups and promising results were obtained. As an example, the research group of CENIMAT already explored some of its properties, but further studies need to be performed. In addition, ZrO_x films with high quality applying a reduced annealing temperature can be reached with adequate metal precursors and solvents and using process engineering (UV post-deposition treatments).

Besides that, it is also important to think in ways to turn laboratories activities safer. Many solvents used every day are toxic and can cause serious harm to human health. With this is mind, the main objective of this work is to produce, study and optimize thin films of zirconium oxide (ZrO_x) by sol-gel method using greener solvents to replace the toxic 2-methoxyethanol (2-ME) and apply these in electronic devices to determine what are the effects of different conditions process on the electrical performance. The final steps are to apply the optimized dielectric layers on flexible substrates and solution-based TFTs developed by the research group of CENIMAT. To reach these final purposes, several tasks were developed:

- Production and characterization of ZrO_x precursor solutions with 2-ME and greener solvents;
- Production and characterization of ZrO_x thin films on silicon and glass substrates deposited by spin-coating and annealed at low temperatures;
- Production and characterization of MIS (Metal-Insulador-Semiconductor) structures using different annealing temperatures and precursor concentrations;
- Production and characterization of metal-semiconductor-metal (MIM) structures on flexible substrates using optimized dielectric films;
- Application of optimized ZrO_x dielectric layers in solution-based TFTs.

This study is an important contribution in the world of the solution processed dielectrics research and a major step closer to the future of flexible and transparent electronics.

1. Introduction

The development of the large area and low-cost electronics required for flat-panel and flexible displays depend heavily on high-throughput fabrication processes and on the characteristics of the selected material. Nowadays, solution-processed amorphous metal oxides are an excellent alternative to physical methods since they present high dielectric constants and no need for vacuum processing conditions. Although the vacuum-based deposition methods (e.g. magnetron sputtering, chemical vapor deposition, atomic layer deposition and e-beam evaporation [1]) have their own advantages, the high fabrication cost restricts the area of application [2]. The use of solution-based procedures, mainly the sol-gel method, present various advantages as low cost, high-throughput and large-area coverage [3]. Furthermore, this method allows to fabricate oxide films with smooth surface morphology and minimal defective sites, which is crucial for ensuring good electrical insulation [4].

Another important characteristic is the use of eco-friendly solvents in the metal oxide precursor solutions, which can minimize the environmental impact resulting from the use of solvents in chemical production.

1.1. High-κ dielectrics

In the past years, the well-established silicon oxide (SiO_2) was the most common material used in the semiconductor industry as insulator in capacitors and transistors. However, with the continuous downscaling was discovered that the silicon-based gate dielectric thickness smaller than 1.2 nm can cause excessive gate leakage current by direct tunneling through the dielectric itself [2]–[5] resulting in power dissipation and heat emission [6]. Therefore, in order to achieve the continuous downscaling and the improved performance of TFTs devices it is necessary to substitute the SiO_2. To reach this purpose several researchers have dedicated research to high dielectric constant (high-κ) materials, such as ZrO_2, HfO_2, TiO_2, Al_2O_3 [7]–[11], because these are suitable to reduce the leakage currents since thicker dielectric layers can be used without altering the required dielectric properties [6] (equation 1) and thus improving the channel modulation in TFTs through reduced tunneling current [12].

The equivalent oxide thickness (EOT) expression corresponds the required thickness of a SiO_2 film that produces the same capacitance value as is obtained when high-κ dielectric is alternatively applied [4], [13]. It is defined as:

$$d_{\mathrm{ox}} = EOT = \frac{3.9}{\kappa} d_{\mathrm{high-}\kappa} \tag{1}$$

where 3.9 is the static dielectric constant of SiO_2, κ is the dielectric constant of a high-κ oxide material, and $d_{\mathrm{high-}\kappa}$ is the thickness of the high-κ dielectric layer.

Among many high-κ dielectrics (Figure 1.1), zirconium oxide has been regarded as one of the most promising inorganic dielectric material because of its excellent properties, including a theoretical high dielectric constant (≅ 25) [3], [6], [14], large bandgap (5.6 eV) [3], [6], relatively low leakage current [15], high breakdown field (≅15–20 MV/cm) [16] and excellent thermal, chemical and mechanical stability with Si [3], [14], [16]. In addition, ZrO_x dielectric can be deposited through a solution-based process, which is a simple method in comparison with vacuum-based deposition methods as atomic layer deposition (ALD) [5].

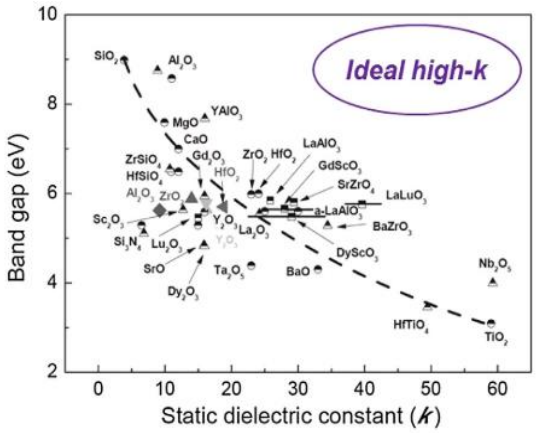

Figure 1.1 - Relation between band gap and dielectric constant for some metal oxide dielectrics [4].

There are few reports on the dielectric properties of solution-processed ZrO_x films. Liu et al. reported the use of UV treatment instead of thermal annealing to produce ZrO_x thin films with a solution using zirconium acetylacetonate in *N*, *N*-dimethylformamide (DMF). A leakage current density of 10^{-9} A cm^{-2} and a high-κ value of 9.8 were achieved [3]. Gong et al. work shows that a low temperature treatment (160 °C) is enough to achieve high quality amorphous ZrO_2 dielectric films via a low-cost solution process, using the same precursor and solvent. The films showed a low leakage current (3.6×10^{-5} A cm^{-2} at -3 V) and dielectric constant of 7.8 [1]. Recently, using a different solvent, 2-methoexyethanol (2-ME), Seon et al. fabricated ZrO_2 films annealed at 300 °C exhibiting a high dielectric constant near 10 and a low leakage current density of 5×10^{-8} A cm^{-2} at an electric field of 1 MV cm^{-1} [6].

1.2. Solution-based TFTs at low temperature

Recently, amorphous thin-film transistors (TFTs) have increasingly been suggested as switching devices for advanced display applications, such as flexible devices, because of their outstanding mobility, exceeds that of amorphous Si-based TFTs, [5], [17]. In addition, solution-derived TFTs have demonstrated impressive performance [1], [15], [18], which in some cases are comparable to or even surpass the ones obtained by physical deposition techniques [5].

Besides the high-throughput and large-area coverage, the low processing temperature is required in the conventional manufacturing process of panel displays [5]. However, for traditional oxide-based TFTs fabricated by solution-processed method, a high temperature is usually required to remove the residual organic species and achieve higher thin film densification [3], [18]. In order to reduce the process temperature and reach similar parameters, solution-processed oxide TFTs have been enhanced by solution (metal precursors, solvents) and process engineering (UV post-deposition treatments) [19]–[21].

As was seen in the sub-section 1.1, solution-based oxide high-κ dielectrics, mainly zirconium oxide (ZrO_x), have been regarded as a promising alternative to the SiO_2 dielectrics due to their high dielectric constant and stable interface chemistry with oxide semiconductors [18] which allow reducing the operation voltage and the power consumption in TFTs [17], [22].

Among various semiconductor channel materials, indium oxide (In_2O_3) has been more utilized due its characteristics, like high electron mobility and high optical transparency in the visible region [18]. Shan et al. demonstrated a fully solution-processed 300 °C annealed In_2O_3/ZrO_x TFT with a μ_{sat} of 13.01 cm^2 V^{-1} s^{-1} and an I_{ON}/I_{OFF} of 1.1×10^7 [23] showing that fully solution-derived oxide TFTs show potential application in portable and low-power consumption electronics. Later, A. Liu et al. fabricated a ZrO_x dielectric thin film using a UV/ozone pre-treatment before the thermal-annealing process and integrated in an In_2O_3 TFT, which exhibited high performances with a μ_{sat} of 23.6 cm^2 V^{-1} s^{-1} and an I_{ON}/I_{OFF} value of 1.1×10^7 [20]. Zhu et al., in a recent report, also fabricated a fully-solution derived In_2O_3/ZrO_x TFTs annealed at 300 °C with a low operation voltage of 2 V, including a μ_{FE} of 4.42 cm^2 V^{-1} s^{-1} and large I_{ON}/I_{OFF} of 7.5×10^7 [18]. Nonetheless, most of the studies reported in literature require high temperature to process ZrO_x thin films for TFT application.

1.3. Eco-friendly solvents

The use of volatile organic solvents (VOSs) are the key to the majority of chemical processes but not without bearing environmental risks. Furthermore, the use of toxic solvents in chemical laboratories and the chemical industry is considered a very important problem for the health and safety of workers. As examples are the 2-methoxyethanol (2-ME) and *N*, *N*-dimethylformamide (DMF) that were used in previous reports about solution-processed ZrO_x dielectric for TFTs application [3], [5], [6], [12], [15] (Table 1.1). These substances present toxicity that is very dangerous for human health, it can cause skin disease and damaged fertility after a long history of exposure. With the aim to reduce chemical related impact on human health and the environment, the minimization of VOSs became a priority in the past years [24].

Novel solvents, such as solvents produced from renewable resources, water, supercritical CO_2 and ionic liquids (ILs), have been proposed in the past decades as "greener" alternatives [25], [26] and they emerge as a replace to the conventional solvents. The idea of "green" solvents expresses the goal to minimize the environmental impact resulting from the use of solvents in chemical production [27]. Furthermore, the solution processing at low temperatures combined with the use of these non-toxic and abundant elements can help minimize fabrication costs and facilitate regulatory acceptance [28].

Table 1.1 - Selected processing details for several reported solution-based ZrO_x deposited by spin-coating ("-" means that the related data is not mentioned in the literature).

Year	**Solvent**	***c*** (M)	**Annealing Temperature** (°C)	t_A (min)	C_i **(nF cm^{-2}) at 1 kHz**	$d_{high-\kappa}$ (nm)	**κ at 1 kHz**	***E*** (MV/cm)	***J*** (A cm^{-2}) **at 1 MV cm^{-1}**
2013 [15]	2-ME	0.3	300	-	~155	120	21	-	-
2014 [29]	DMF	0.1	UV assisted	30	~750	5.5	~9.5	9.5	~1 × 10^{-9}
2015 [3]	DMF	0.1	150	33	~302	14.6	~6.2	7.7	~7 × 10^{-9}
2016 [5]	2-ME	0.2	350	120	138	139	21.7	-	-
			250	120	97	143	15.7	-	-
2017 [30]	Ethanol	0.2	UV assisted	80	~750	-	~12	-	-
2017 [2]	2-ME	0.3	400	-	300	66.9	15-22	-	-
		0.1	400	-	760	22.5	15-22	-	-
2018 [18]	2-ME	0.1	400	60	313	18.8	5.7	-	~9 × 10^{-10}
		0.1	300	60	388	18.3	7.1	-	~9 × 10^{-10}
2018 [6]	2.ME	-	300	60	-	150	~10.5	> 4	5 × 10^{-8}
2018 [1]	DMF	0.15	300	60	219	40.3	8.8	-	-
			160	60	117	59	7.8	-	-

The table above exhibit the results obtained for several reported solution-based ZrO_x dielectrics using different types of solvents. The 2-ME and DMF are the most used solvents and only one article published in 2017 studied the advantages of ethanol as solvent. Among various "greener" solvents, ethanol is the most environmentally favourable solvent according to the environment, health & safety method (EHS) and the life-cycle assessment method (LCA). It has low toxicity, low EHS score and it derived from renewable sources [31].

1.4. Metal-Insulator-Semiconductor capacitors

The capacitor is one of the three basic passive circuit components of any electronic or electrical circuit. It gets charged when a steady voltage *V* is applied and keeps energy even after removal of external voltage [32]. This passive component can have different structures but the most common is built out of two parallel metal electrodes separated by a thin dielectric (or insulator) layer, which is usually a solid or a paste but may be liquid, gel, gaseous, or vacuum [33]. The conductive plates are oppositely charged (+Q at one plate and -Q on the other) and when the capacitor is disconnected from the power source, the opposite charges on its plates will persist in equilibrium as a result of their mutual attraction [33].

The stored charge is measured in *coulomb* and is given by $Q = CV$, where V is the potential difference applied between the plates and by the capacitance (C; F). On its turn, the capacitance is a measurement of the ability of a capacitor to store electric charge and it is defined by Faraday for a pair of plates by equation 2 [13]. It depends on the electrode area (A; m^2), permittivity of vacuum (ε_0; 8.85 × 10^{-12} F m^{-1}), dielectric constant (κ) and thickness of the material (d; m). An ideal metal-insulator-metal (MIM) capacitor will not dissipate any power and will have a constant capacitance, but a real capacitor consumes a small amount of power whenever current flows through it, due to ohmic losses, which are minor at supply frequencies but can get significant at higher frequencies, depending on the type of capacitor [32].

$$C = \varepsilon_0 \kappa \frac{A}{d} \tag{2}$$

The metal-insulator-semiconductor (MIS) capacitor consists of two metal electrodes as the MIM capacitor, however, it contains one more layer, a semiconductor layer between the bottom electrode and the dielectric layer (Figure 1.2 a)). The oxide functions as the dielectric and the area of the metal gate defines the area of the capacitor. Its structure is present in MIS field-effect-transistor, such as MOSFETs. The first one was made of SiO_2 grown thermally on silicon surface and this immediately led to the first report of MOSFET [34]. The particularity of these electrical devices is that the Faraday formula cannot be applied in them. Different from MIM capacitors, their capacitance changes with a DC voltage applied on the gate due to the semiconductor presence.

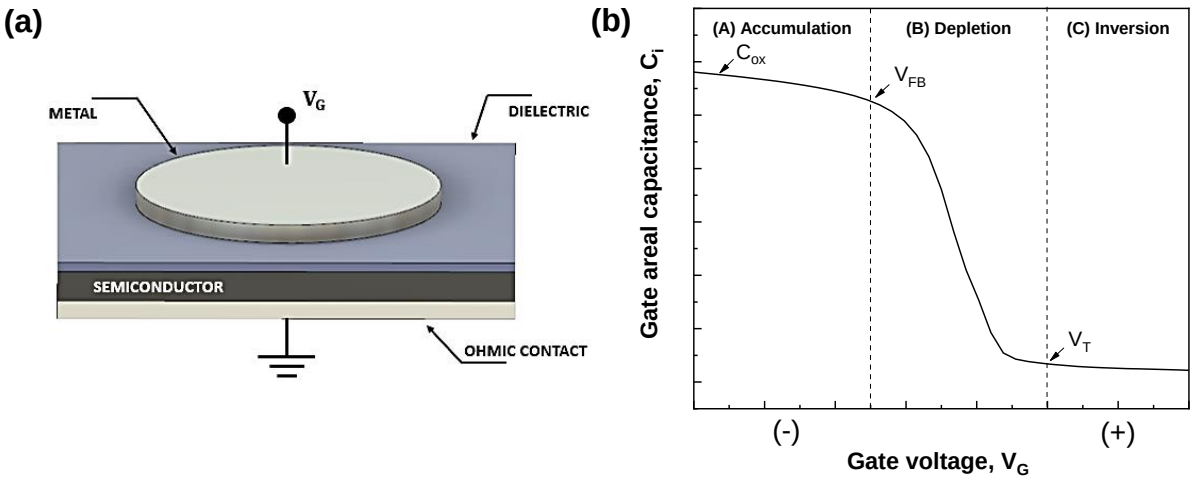

Figure 1.2 – (a) Schematic representation of a MIS capacitor device, where V_G is the applied voltage. (b) Theoretical $C - V$ curve of a p-type MOS capacitor at high frequency.

Considering a MOS structure with a p-type Si substrate and a top metal gate as show in Figure 1.2 a), the gate capacitance per unit area (C_i) can be conveniently expressed as a series combination of the oxide capacitance (C_{ox}) and the Si surface capacitance (C_s) [35]:

(3)

$$\frac{1}{C_i} = \frac{1}{C_{ox}} + \frac{1}{C_s}$$

The Si surface capacitance, C_s, is a measurement of surface charge density responding to the charge of surface potential. The oxide capacitance, C_{ox}, is fixed, but the gate voltage changes the surface potential and this in turn changes the gate capacitance [35]. To determine the capacitance value in MOS capacitors, the characterization is done with the capacitance-voltage ($C-V$) curves. As a voltage sweep is applied to the gate, it causes the device to pass through accumulation (A), depletion (B), and inversion regions (C) (Figure 1.2 b)); which are described below. The two voltages that determine the three regimes are (a) flat band voltage (V_{FB}) (the gate voltage at which there is no charge in the MOS capacitor) which separates the accumulation regime from the depletion regime and (b) the threshold voltage (V_T) which determines the depletion regime from the inversion regime [36].

(A) Accumulation region ($V_G < V_{FB}$): As the gate voltage (V_G) takes large negative values, the number of negative charges induced on the gate increase attracting majority carriers (holes) to the silicon surface. The hole concentration at the surface is above the bulk value forming an accumulation layer. In this region, the total capacitance (C_i) approaches the capacitance of the oxide film (C_{ox}) since the contribution of si surface capacitance (C_s) to the total capacitance is negligibly small; $C_i = C_{ox}$. [35]–[37]

(B) Depletion region ($V_T > V_G > V_{FB}$): When V_G increases towards positive values, holes are repelled from the silicon surface to balance the gate charge. This area of the semiconductor acts as a dielectric because it can no longer contain or conduct charge. The contribution of C_s can not be neglected in this region because the depletion width increases with the increasing surface potential. Thus, the total capacitance (C_G) is measured by the oxide capacitance in series with Si surface capacitance (C_s), $C_i = C_{depletion} = \frac{C_{ox} C_s}{C_s + C_{ox}}$, and decreases until the threshold voltage (V_T) is reached. [35],[36]

(C) Inversion region ($V_G > V_T$): As the V_G increases beyond the threshold voltage (V_T), electrons appear at the silicon surface in great numbers forming an inversion layer (i.e., n-type channel). When MOS capacitor is at high frequency (f) and above a certain positive gate voltage, these minority carriers cannot be generated fast enough and further gate-voltage increases do not further deplete the semiconductor. In this case the gate capacitance (C_i) decreases to a minimum value as the silicon depletion layer approaches its maximum width, and the corresponding minimum surface capacitance $C_s = C_D(\min)$; $C_i = C_{depletion,min} = \frac{C_{ox} C_D}{C_D + C_{ox}}$. [35],[36]

In this work, we report the use of 2-ME or Ethanol as solvent in zirconium-based solutions to fabricate dielectrics films at low temperature and the application of these films as capacitor dielectrics and gate insulators in In_2O_3 TFTs. For the first time, a comparision is perfomed between devices fabricated with a toxic and a green solvent and with 0.1 M and 0.2 M precursor concentration. Futhermore, different from the published works, a thermal annealing is applied at the same time with UV irradiation (DUV ou FUV) for faster film densification. Some results obtained even surpass the state-of-the-art depicted in Table 1.1.

2. Materials and Methods

The ZrO_x thin films were produced by a solution deposition technique, spin coating. Different annealing temperatures, precursors, solvents and molar concentrations were tested. In order to determine the optimized dielectric, we fabricated MIS capacitors. Then, a MIM capacitor was produced on flexible substrate with the dielectric that showed better characteristics. Finally, ZrO_x thin films were used as insulator gate in solution-based In_2O_3 TFTs.

2.1. Fabrication of ZrO_x thin films by solution processing

The precursors solutions were prepared by dissolving zirconium oxynitrate hydrate ($ZrO(NO_3)_2 \cdot xH_2O$, ALDRICH, 99%) in 2-methoxyethanol (2-ME, $C_3H_8O_2$, ACROS Organics, 99% or Fisher Chemical, ≥ 99%) or in ethanol absolute anhydrous (CH_3CH_2OH, CARLO ERBA, ≥ 99.5%) at a concentration of 0.2 M and 0.1 M. The solutions were stirred continuously for 2 h under ambient conditions. In the solution with 2-ME as solvent a fuel, urea ($CO(NH_2)_2$, Sigma, 98%) (not soluble in ethanol), for combustion reaction was added and stirred continuously at least 1 h. The molar proportion between urea and the zirconium oxide reagent was 5:3 to guarantee the redox stoichiometry of the reaction (Annex A). For convenience, the solution with urea is called, here after, ZrO_x U.

Prior to the deposition of ZrO_x thin films, the 2.5 x 2.5 cm p-type single crystal 100-oriented silicon (resistivity ≅ 1-2 Ω · cm) and the glass substrates were cleaned by immersing for 10 min in acetone at an ultrasound bath at 60 °C. This procedure was repeated with IPA and then, the substrates were thoroughly cleaned in deionized water and dried by nitrogen flow subsequently. In order to enhance the adhesion properties of the thin films on the substrate, the substrates were exposed to UV-ozone treatment (Novascan PSD-UV) for at least 15 min at a 5 cm distance of the UV lamp. The precursor solutions were filtered through a 0.22 µm polytetrafluoroethylene (PTFE) syringe filter before solution casting. The ZrO_x solution was then spun on the Si/Glass substrates at a speed of 2000 rpm for 35 s. After that, the thin films were finally annealed on a hot plate, to evaporate the solvent and improve the densification, at different conditions: (i) annealed at 150 °C on hot plate with a short-wavelength deep ultraviolet (DUV) photochemical activation with a mercury lamp (main peaks at 184.9 nm (10%) and 253.7 nm (90%)) for 30 min in N_2 condition; (ii) annealed at 150 °C on hot plate and under DUV lamp for 1 h in N_2 condition; (iii) annealed at 250 °C on hot plate for 30 min; (iv) annealed at 300 °C on hot plate for 30 min; (v) annealed at 350 °C on hot plate for 30 min. The distance between DUV lamp and thin films was kept at 2 cm. For convenience, the thin films annealed by different times and temperatures are called, hereafter, X – 150 + DUV, X – 250, X – 300, X – 350, with “X” corresponding to the respective solvent name.

2.2. Fabrication of MIM/MIS capacitors

In order to determine the optimized thickness and annealing temperature of the ZrO_x thin films, MIS capacitors (Al/ZrO_x/p-Si) were fabricated. A simplified diagram to obtain the MIS devices is presented in Annex B – Figure 6.1 as well as the process steps. The ZrO_x capacitors were finalized by thermal evaporation of a 80 nm aluminium (Al) bottom electrode on the Si substrate for optimize the ohmic contact and 80 nm Al top electrodes using a circular shadow mask (Annex B - Figure 6.1 d)), which produced capacitors with different areas (0.2 mm^2, 0.8 mm^2 and 3.1 mm^2).

With the optimized ZrO_x thin film condition, a similar procedure was performed to produce MIM capacitors (Au/ZrO_x/Al) on flexible substrates (Annex B – Figure 6.2). A 2.5 x 2.5 cm Kapton was cleaned with ethanol and dried under nitrogen flow subsequently. Before the deposition of the bottom electrode (80 nm Al) by thermal evaporation, a UV-ozone treatment was applied for 15 min. Then, to avoid substrate shrinking during the thin film deposition, a 180 °C thermal annealing was applied for 10 min. The spin coating was also used for thin film deposition. In this case, 2 layers were deposited with an annealing temperature of 150 °C + DUV for 1 h. The UV-ozone surface activation step was also used between layers deposition for 10 min. A 80 nm thick gold (Au) top electrode was deposited by e-beam evaporation on the clean zone. A titanium (Ti) layer was first deposited to ensure the Au adhesion and to better electrical performance.

2.3. Production of solution-based oxide TFTs

Finally, TFTs were produced to investigate the application of high-κ ZrO_x gate dielectrics in solution-processed In_2O_3 TFTs. The In_2O_3 active layer was deposited using spin-coating at 500 rpm for 5 s as initial step and at 8000 rpm for 60 s as second step. Both layers were annealed at the same temperature and time in 2 conditions: (i) 200 °C on hot plate and under far-ultraviolet (FUV) lamp (H2D2 light source unit, model L11798; main peak at 160 nm) at a distance of 5 cm for 30 min in N_2 condition and (ii) 300 °C on hot plate for 30 min. Finally, 80 nm thick Al source/drain (S/D) electrodes were thermally evaporated on the active layer through a shadow mask to produce a channel width (W) of 1400 µm and a channel length of (L) 100 µm. The 80 nm thick Al gate was also deposited by thermal evaporation.

2.4. Microstructure investigation and characterization of electrical properties

To study the produced thin films, various characterization techniques were used. To measure the organic bonding states the Fourier-transform infrared spectroscopy (FT-IR, Nicolet 6700) was used in absorbance mode. The FTIR was equipped with an attenuated total reflectance (ATR) sampling accessory and all spectra were obtained after the correction of the atmosphere contribution. The optical properties of films spin-coated on glass were measured by an UV-Vis-NIR Spectrophotometer (Perkin Elmer Lambda 950) in the 200-800 nm range. The surface morphology of thin films were investigated by optical microscope (Olympus BX51) and atomic force microscopy (AFM, Asylum MFP3D) was used to investigate the roughness of kapton substrate. The thickness of ZrO_x thin films on silicon (Si) substrates were evaluated by spectroscopic ellipsometry (UVISEL Plus ellipsometer). The thermogravimetry and differential scanning calorimetry (TG-DSC, STA 449 F3 JUPITER) were used to identify the thermal behaviour of the thin films precursor solution, the experiments were carried out in a synthetic air atmosphere up to 550 °C with a heating rate of 20 K/min using xerogel solutions. The crystal structure of a ZrO_2 powder was analysed by X-Ray Diffractometer (XRD, X'Pert PRO PANalytical) at 45 kV and 40 mA equipped with a Cu Kα source (λ = 1.540598 Å). The crystallinity of ZrO_x thin films deposited on silicon substrate followed by thermal annealing at 350 °C were also investigated through the same XRD in grazing incidence mode (GIXRD, X'Pert PRO PANalytical) using the same measurement conditions and an angle of incidence of the X-ray beam fixed at 0.5°.

The electrical and dielectric properties ($C-V$, $I-V$ and $C-f$ measurements) of the MIS/MIM capacitors ZrO_x-based were investigated using a semiconductor parameter analyser (Keysight B1500A) with a probe station (Cascade EPS150 Triax). Also, the electrical performance of the TFTs (Al/In_2O_3/ZrO_x/p+-Si) was evaluated by measuring the transfer curves ($I_D - V_G$) using the same equipment.

3. Results and Discussion

The results obtained for the precursor solutions characterization, thin films characterization and electrical characterization of MIS/MIM capacitors and TFTs are analysed in this chapter.

3.1. Precursor solutions and powder characterization

All results presented in this sub-chapter refer to the ZrO_x precursor solution with a zirconium nitrate molar concentration of 0.2 M.

3.1.1. Precursor solutions characterization

Figure 3.1 shows thermogravimetry (TG), and differential scanning calorimetry (DSC) results for the ZrO_x xerogels produced with different solvents (2-ME and ethanol absolute). Figure 3.1 a) exhibits an intense exothermic peak at 76 °C with corresponding abrupt mass loss (34.69 %), which is caused by the degradation of residual organics. A regular mass loss of 11.75 % is observed up to 100 °C. No significant chemical reactions were observed above ≅ 350 °C, implying that the thermal reaction and the alloy mechanism were almost complete during annealing process at temperatures above ≅ 350 °C [1].

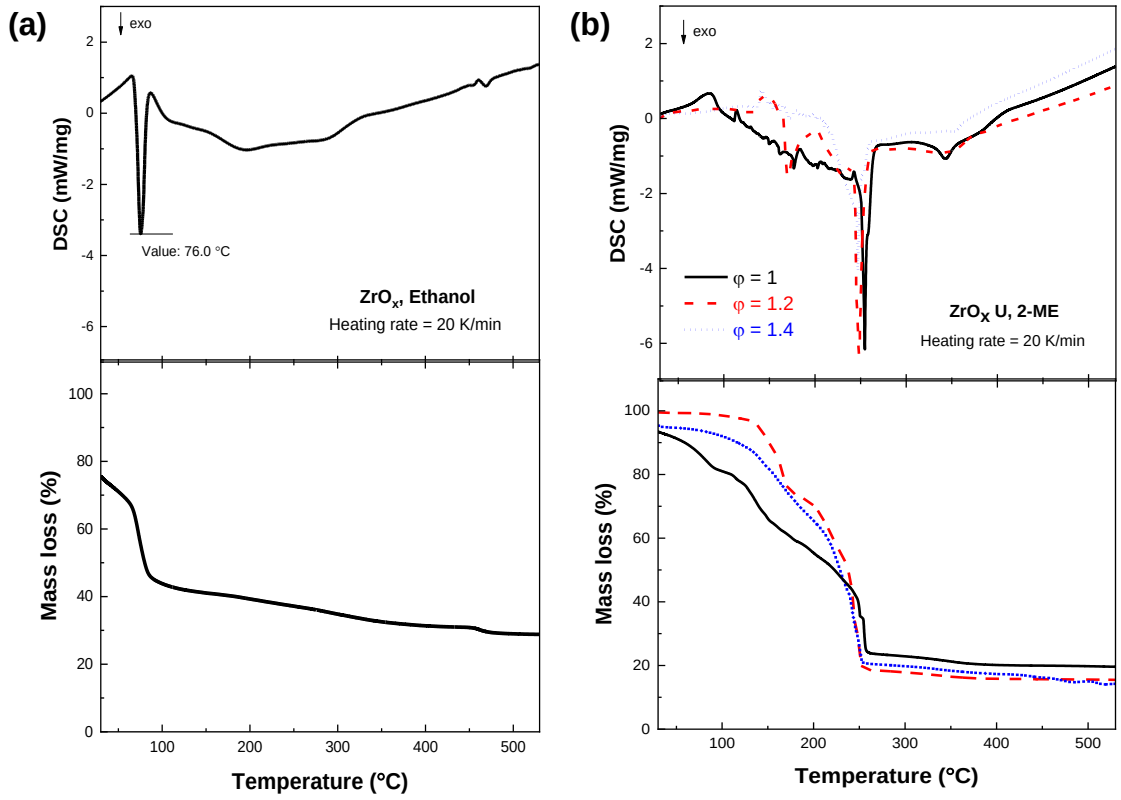

Figure 3.1 - Thermal analysis (TG-DSC) of ZrO_x xerogels produced with: (a) ethanol absolute or (b) 2-methoxyethanol (2-ME) as solvent.

In the case of the xerogel solution using 2-ME as solvent and urea as fuel (3.1 b)), solutions with different equivalent ratios (ϕ) were studied (1, 1.2 and 1.4) using the same heating rate of 20 K/min. The ϕ = 1 plot shown an intense exothermic peak at 254.6 °C (40.96 %), which is caused by the exothermic combustion reaction of the organic fuel with the zirconium nitrate. Regular weight losses are observed before this peak (13.27 % and 16.53 %) followed by endothermic peaks indicating the

solvent evaporation. A small exothermic peak is observed at ≅ 345 °C, which indicates the still existence of residual organics in the xerogel. No apparent mass loss is observed at temperatures above ≅ 350 °C, which indicates that the xerogel was converted into ZrO_x metal oxide completely [2]. Increasing the number of moles of fuel in the solution, the exothermic peak shifts further to the left. The ϕ = 1.2 and ϕ = 1.4 plot shown an intense exothermic peak at 248 °C and 247 °C, respectively, a variation of ≅ 3% compared with φ = 1 xerogel. As the changes in the peak are negligible, we use the solution with a balanced stoichiometry to produce all dielectric films.

The study of the solution with urea (Combustion method) and without was reported in other works [19], [38]. The additional energy provided by the exothermic combustion reaction, that occurs using a fuel (urea) and an oxidizer (nitrate ions), contributes to remove organic residuals and enhance film densification, M-O-M formation, in a short annealing time. To obtain high quality ZrO_x films at low temperatures, the use of urea as fuel in 2-ME was essential in this work.

3.1.2. Powder characterization

A ZrO_2 powder was obtained by conventional combustion method (CCM) with a 10 ml solution using zirconium oxide nonahydrate and urea as precursors and 2-methoxyethanol (2-ME) as solvent. The solution was taken in an alumina crucible and treated in an air furnace at 300 °C for 1 h. To determine the crystallinity of it, an XRD pattern was obtained and it is shown in Figure 3.2.

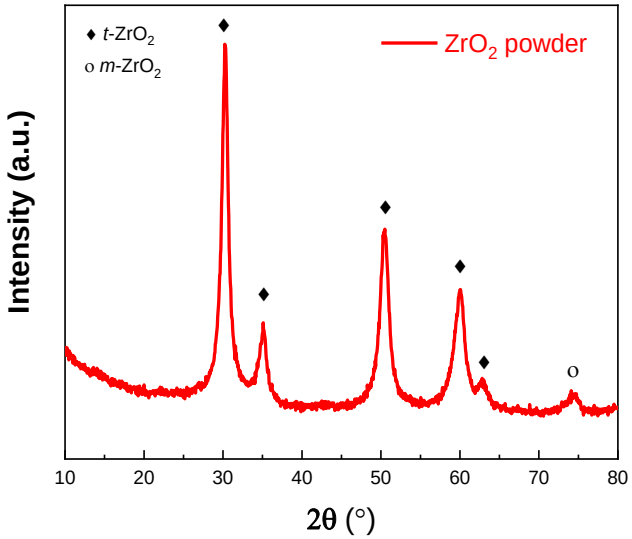

Figure 3.2 - XRD pattern of ZrO_2 powder obtained by conventional combustion method (CCM). **Notes**: o, monoclinic phase; ♦, tetragonal phase of zirconia.

Obvious diffraction peaks are observed at the crystal powder. The ZrO_2 can exists in three major crystal phases: cubic, tetragonal, and monoclinic polymorphs [6], the crystallization phase depends upon the temperature conditions employed during the synthesis and the time of the reaction [39]. In order to determine the crystalline phase or phases presence in the ZrO_2 powder, we must determine the position and the d-spacing values of the observed diffraction peaks (Table 3.1). The first 5 peaks are associated with [111], [200], [220], [311] and [222] planes and can be readily assigned to a tetragonal phase of ZrO_2 [2], [39]. The peak at 75.1° can be assigned to a monoclinic phase [40], [41]. Furthermore, no characteristic peaks from other crystalline impurities were detected by XRD, suggesting the high purity of ZrO_2 polycrystalline.

Table 3.1 - Peaks position (°), d-spacing values (Å) and relation intensity (%) of the diffraction peaks exibited in the Figure 3.2.

2θ (°)	d-spacing (Å)	Crystal phase
30.24	2.95	Tetragonal
35.00	2.55	Tetragonal
50.57	1.81	Tetragonal
58.89	1.53	Tetragonal
62.85	1.48	Tetragonal
75.10	1.54	Monoclinic

3.2. Thin films characterization

The XRD and TG-DSC results presented in this chapter refer to thin films fabricated with a ZrO_x solution with a zirconium nitrate molar concentration of 0.2 M except for spectroscopic ellipsometry results where solutions with 0.1 M and 0.2 M were studied.

3.2.1. Structural Characterization

Above a certain annealing temperature, the solution-processed ZrO_x thin films can show a crystalline phase. The crystallization in dielectric films can provide pathways for leakage current due to the grain boundaries, leading to a large leakage current and a small on/off ratio resulting in a poor TFT performance [2]. On other hand, amorphous thin films exhibit a lot of advantages, including smooth surface, high stability, low interface state density and large-area uniformity [23], which eliminates some of the problems associated with crystalline films.

To determine the crystallinity of the spin-coated thin films, the XRD technique was performed in grazing angle mode for thin films annealed at the highest temperature (350 °C). Different from the powder analysis in the section 3.1.2, it can be seen in the XRD patterns (Figure 3.3) that both ZrO_x thin films are amorphous; the diffraction peaks at 2θ= 51.4° and at 2θ= 53.4° followed by a bump are forbidden peaks of 100-oriented silicon wafer that appear when the grazing angle mode is used at certain phi angle [42]. This can be explained by the fact that the ZrO_2 powder was fabricated with 0.2 M precursor concentration and all the 10 mL solution was introduced in the oven to produce it. In the spin-coating system, using a syringe with 5 mL of solution, only a small amount of solution, and precursor as well, is deposited on the substrate surface to form the thin film. In conclusion, the formation mechanism to form the thin films is different when compared with the powder mechanism.

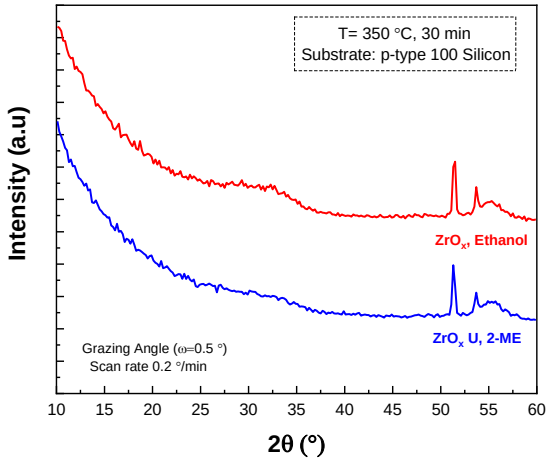

Figure 3.3 - Grazing incidence XRD patterns of the spin-coated thin films annealed at 350 °C using different precursors solutions deposited on silicon: zirconium nitrate with urea (U) and 2-ME as solvent (blue curve) and zirconium nitrate with ethanol absolute as solvent (red curve).

Through optical microscope analysis, the morphology of the thin films surface could be confirmed intuitively, and a comprehensive conclusion could be made comparing with the crystallographic analysis of XRD. As expected, the condition of 350 °C show microscopically flat surfaces (Annex C).

3.2.2. Chemical Characterization

In order to understand the formation processes of the ZrO_x thin films under annealing conditions, ATR-FTIR measurements were carried out on zirconium oxide coatings on silicon substrate with different processing conditions (Figure 3.4 and 3.5).

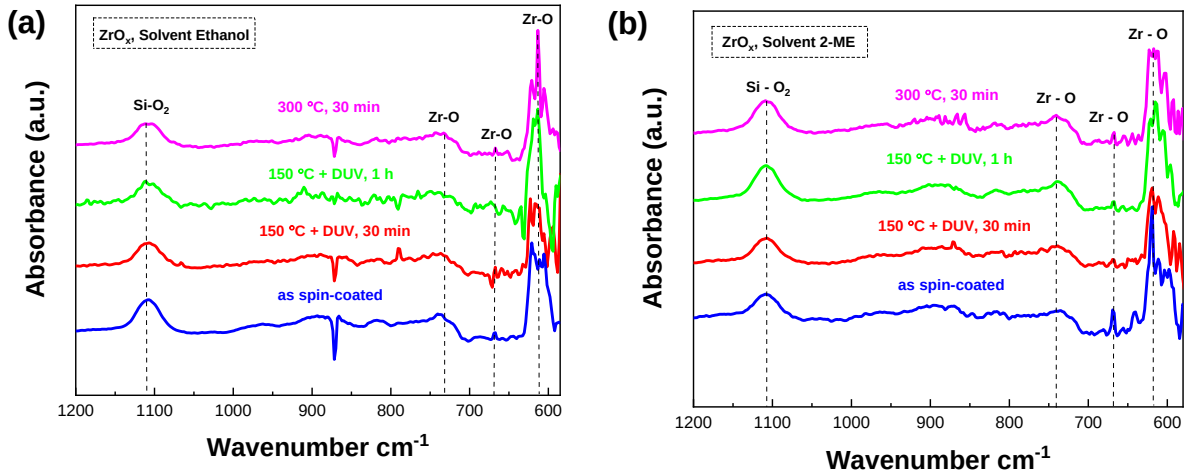

Figure 3.4 - FTIR analysis at 580-1200 cm^{-1} range of the ZrO_x thin films produce (a) with ethanol, (b) 2-ME as solvent under various annealing conditions.

The infrared absorption spectra at 525–1200 cm^{-1} range (Figure 3.4) show a band approximately at 1100 cm^{-1}. It is associated to the asymmetric stretching vibration of the native SiO_2 layer (1-2 nm) present at the interface of the silicon substrate [43], [44] . The peaks approximately at 610, 667 and 740 cm^{-1} are from Zr-O vibrations [45]–[47].

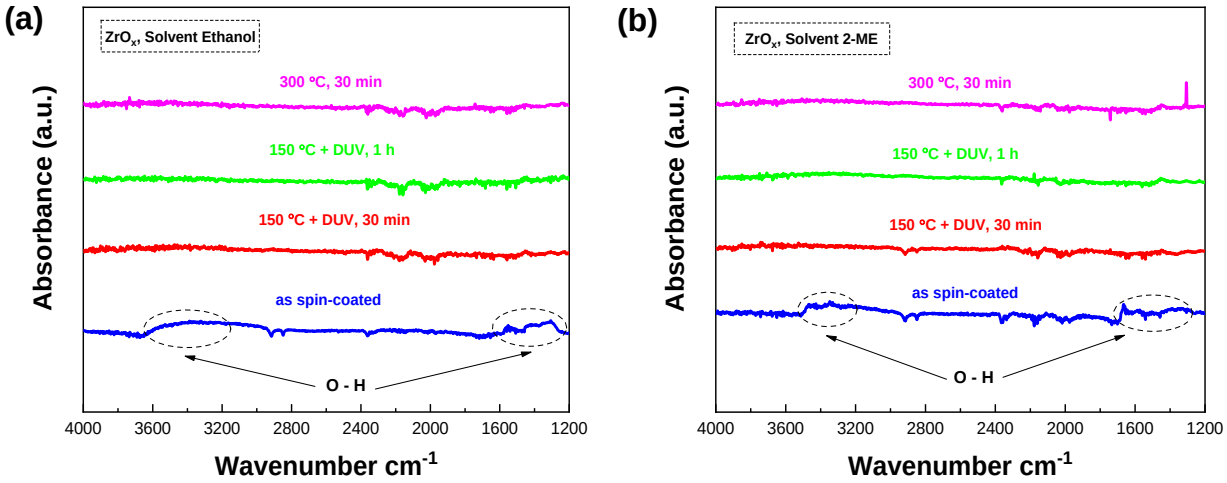

Figure 3.5 - FTIR analysis at 1200-4000 cm^{-1} range of the ZrO_x thin films produce (a) with ethanol, (b) 2-ME as solvent under various annealing conditions.

In the Figure 3.5 the spectra at 1200–4000 cm^{-1} range are shown. Several vibration peaks were observed in ZrO_x xerogel films without annealing treatment. The peaks observed around 3200-3600

cm^{-1} are attributed to the OH stretching vibrations of water molecules, indicating a higher amount of surface hydroxyl groups [39], [44], [45], [48]. The absorption bands located between 1300 and 1700 cm^{-1} are associated with their bending mode [39], [43]–[45]. These bonding suppress the condensation of the metal oxide gel films by chelating with coordination bonding to the metal ions [23]. During the thermal annealing step, the groups were gradually separated, and decomposed, and only trace amount of vibration peaks can be observed in the FTIR analysis, when compared with the as spin-coated film.

The FTIR results in the 600 to 1200 cm^{-1} range exhibited the presence of Zr-O, ligands in the film, resulted from the film densification. The 1200 to 4000 cm^{-1} range indicates that the annealing process is fundamental to obtain solution-based thin films with high quality. This step can effectively reduce the residual organic components in the gel films and promote the condensation/densification of them forming more Zr-O ligands.

3.2.3. Optical Characterization

The spectral transmittance curves with the wavelength ranging from 200 to 800 nm for two solutions deposited on glass substrates: zirconium nitrate with urea (U) and 2-ME as solvent and zirconium nitrate with ethanol absolute as solvent are shown in Figure 3.6. For each solution, thin films with different annealing temperatures were produced, measured and demonstrated with different line colours.

It is found in the 2-ME plots (3.6 b)) a transmission between ≅ 85 % and ≅ 91 % in the visible light range (400-800 nm). In the ethanol plots (3.6 a)) is observed a transmittance between 81% and 90%. These high transparency over 80% for the entire visible light region indicates the potential applications of the devices in transparent electronics [18].

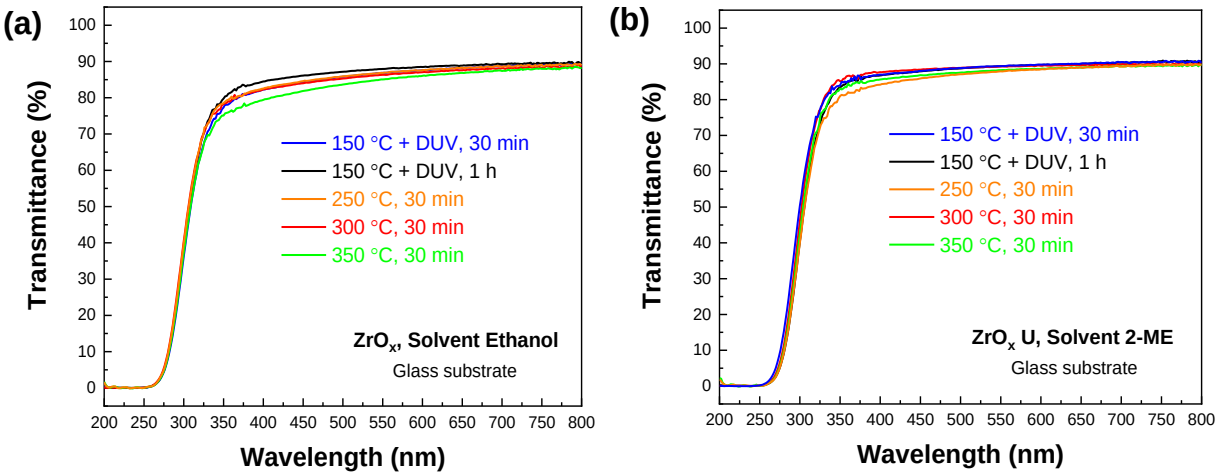

Figure 3.6 - Optical transmittance of ZrO_X thin films produce (a) with ethanol, (b) 2-ME as solvent under various annealing conditions.

The thickness of the thin films fabricated at different conditions were evaluated using an ZrO_X spectroscopic ellipsometry model developed at CENIMAT (Figure 3.7).

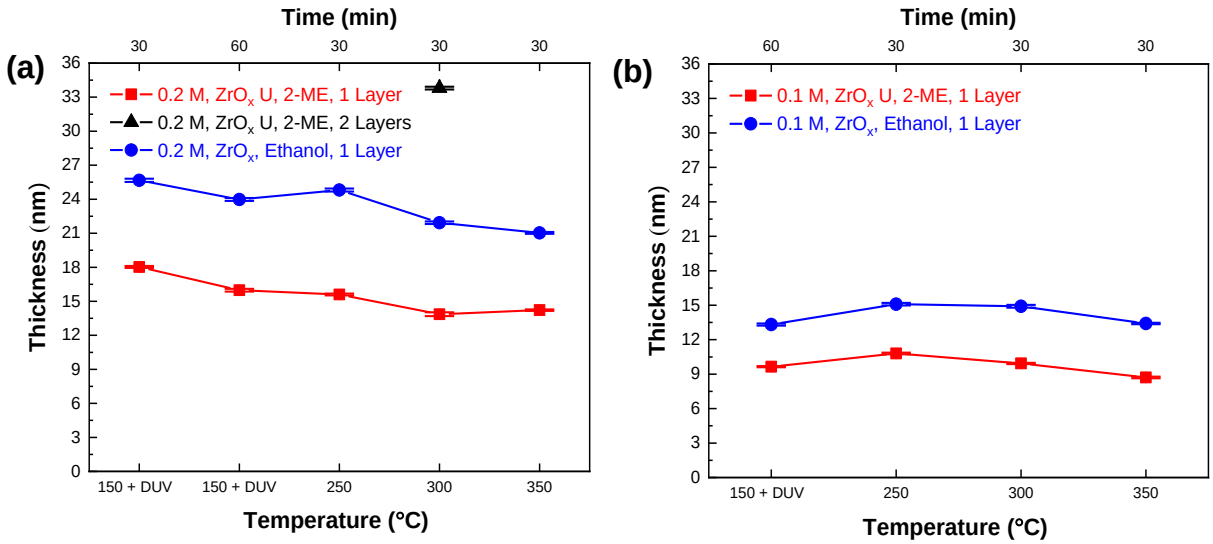

Figure 3.7 - Thickness of ZrO_X thin films produced with (a) 0.2 M precursor solutions, (b) 0.1 M precursor solutions with ethanol and 2-ME as solvents at different temperatures and times.

The data in the Figure 3.7 a) show that the ethanol films exhibit higher thickness than 2-ME films for all the submitted conditions. Due to equipment limitations it was not possible to measure the viscosity of the solutions, but a higher viscosity of the ethanol solution may be the explanation of the higher thickness obtained for these films. As presented in the TG-DSC results, the film densification increases with increasing temperature, due to this it can also be seen a decrease trend with increasing temperature in the Figure 3.7. However, Ethanol-150 °C for 1 h shows lower thickness than Ethanol-250 °C because the DUV treatment combined with low temperature helps in the film condensation and densification.

If the number of layers deposited increased, the film became thicker as expected. Using 2-ME, a 0.2 M solution was produced, and two ZrO_X layers were deposited on silicon (Si). The standard temperature (300 °C) was used to the annealing step. The thickness obtained for the 2 layers was 33.8 ± 0.1 nm, slightly higher than two times the 13.9 ± 0.2 nm obtained for 1 layer (Annex D).

Dielectric films with 0.1 M precursor concentration were also produced to compare the electrical properties with 0.2 M films (Figure 3.7 b)). They exhibited a lower thickness for all conditions, which means that dielectric thickness decreases by decreasing the concentration.

Also, with the ellipsometry measurements was possible to obtain the films optical band gap (Figure 3.8)

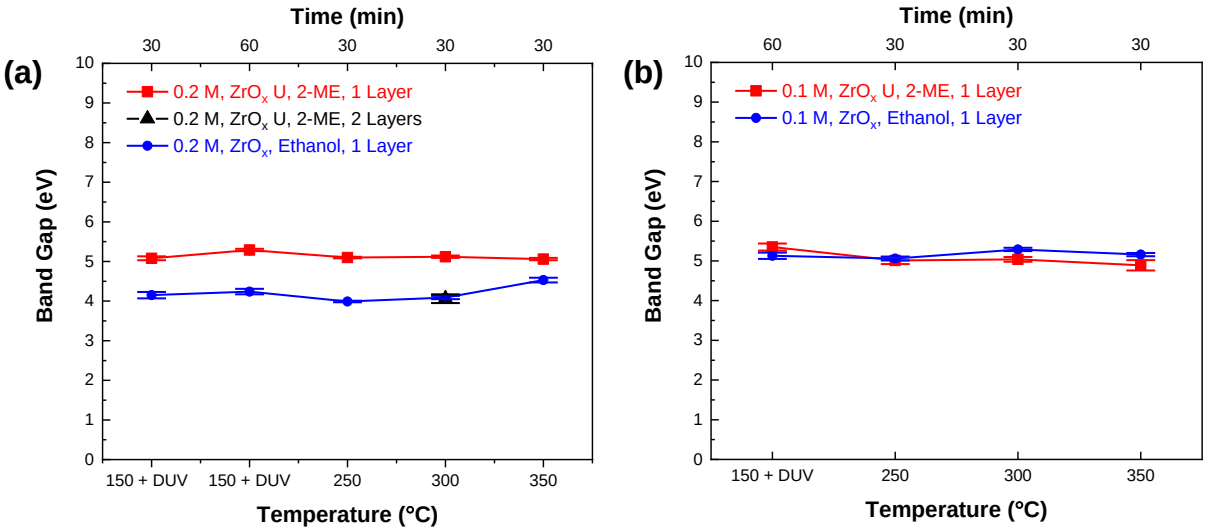

Figure 3.8 - Band gap of ZrO_x thin films produced with (a) 0.2 M precursor solutions, (b) 0.1 M precursor solutions with ethanol and 2-ME as solvents at different temperatures and times.

For the 0.2 M films (Figure 3.8 a)), the values obtained for the solution with ethanol as solvent were between 4.0-4.5 eV and between 5.1-5.3 eV for the solution with 2-ME (Annex D). For the 2-ME-2 layers condition, a band gap of 4.1 ± 0.1 was obtained. When compared with 0.1 M films (Figure 3.8 b)), the band gap values of ethanol solution-based films are lower for all the conditions. On other hand, for 2-ME solution-based films the values are similar. Previous reports stated that photonic properties of thin films depends on the particle size. [49]–[51] In other words, the increase in band gap with decrease in the precursor concentration or number of layers is the quantum confinement effect manifested by the decreasing size of ZrO_x particles.

Slightly higher values, more approximate to the theorical value ($ZrO_x \cong 5.6$ eV), were obtained for reported ZrO_x solution-based thin films [1], [18]. However, they used other methods instead of ellipsometry measurements. As a next step to continue this work, UV-Vis measurements in thin films deposited on quartz substrate should be performed.

3.3. Eletrical characterization of solution-based capacitors

The quality of TFTs is highly dependent on characteristics of the insulating material and the properties of insulator-semiconductor interface. For this reason, the insulating layer has been studied using metal-insulator-semiconductor (MIS) structures. The electrical characterization of the capacitors is done using three curves: areal capacitance-voltage ($C - V$), areal capacitance-frequency ($C - f$) and current-voltage ($I - V$). They enable to obtain important parameters to characterize and analyse different dielectric layers.

The $C - V$ curves show hysteresis in a clockwise direction for all the processing temperatures, which is assigned to the trapping of charges in the dielectric layer or at the interface [38]. The $C - f$ curves allow to see the changes of capacitance with the frequency (in a range of 1 kHz to 100 kHz) to different applied voltages and the $I - V$ curves enable to determine the current behavior when it passes through the device according to the voltage applied to the gate. Dividing the current by electrode area and the applied voltage by dielectric thickness is possible to obtain the density current-electric field ($J - E$) curve, where we can extract the minimum electric field value necessary to the capacitor become a conductor.

The capacitors with small area ($\cong 0.2$ mm^2) were chosen to be measured in all devices because it was seen by microscope that these presented better conditions, as uniformity. Different capacitors produced in the same synthesis conditions were measured and the figures in the next sections show the values average (more than 6 devices) of those with better electrical performance.

The frequency chosen to measure the capacitance of the dielectrics was 1 kHz to have all the dielectrics in the same condition because in certain cases the areal capacitance decrease with higher frequencies, which can be attributed to the limited polarization response time [18].

3.3.1. Influence of precursor reagents and solvents

As discussed in the section 1.2, with the increasing of environmental concern, the principles of green chemistry, which guide us to use safer and more environmentally friendly solvents, are becoming extremely important. Having that into account, other solvents were tested in this work to substitute the well-known 2-methoxyethanol (2-ME). One of these solvents, the ethanol absolute, one of the most environmentally solvent was used successfully in this work. The deionized water (H_2O), 2-Methoxy-1-propanol ($C_4H_{10}O_2$) and 1-butanol ($C_4H_{10}O$) are also "greener" solvents [52] than 2-ME and were also tested as solvents in solutions. Unfortunately, the zirconium nitrate precursor is not soluble in 2-methoxy-1-propanol or 1-butanol and so it was not possible to obtain a transparent solution. On other hand, using deionized water as solvent a transparent solution was obtained but the MIS devices fabricated with this solution showed a conductor behaviour possible due to the lower thickness and existence of pinholes.

In the figures below we can compare the results obtained for capacitors fabricated with different solutions: i) zirconium nitrate and urea (U) as fuel in 2-ME (Combustion method) and ii) zirconium nitrate in ethanol (Sol-gel method).

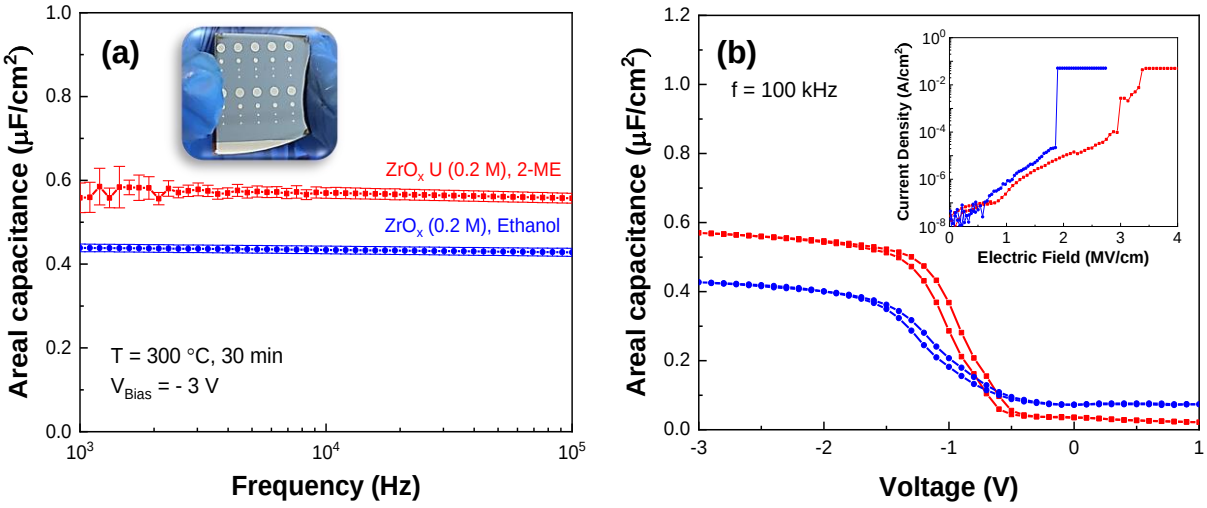

Figure 3.9 – Characteristic curves of 2-ME and ethanol solution-based Al/ZrO_x/p-Si capacitors annealed at 300 °C and with an area of 0.2 mm^2: a) Capacitance-frequency and in the inset an image of the MIS structure fabricated and b) Capacitance−voltage to a frequency of 100 kHz with current density-electric field curves in the inset.

The 2-ME-300 capacitors exhibit a higher capacitance per unit area (C_i), between 1 kHz and 100 kHz, than Ethanol-300 capacitors (as expected by the equation 2). In addition, the both MIS structures show a small variability of capacitance with frequency (≅ 3 %) (Figure 3.9 a)), which indicates a low defect density of the thin films. The figure 3.9 b) presents the average capacitance *versus* voltage and the leakage current density at various electric fields for the same capacitors. They both exhibit a small width hysteresis indicating a small quantity of charges trapped on dielectric layer or at interface. The leakage currents densities at 1 MV cm^{-1} are low for both devices and it is slightly better for the 2-ME solution-based capacitors (Table 3.2). These results demonstrate the possibility for the applicability of gate insulators in solution-based TFTs.

The dielectric constants (κ) of the materials (Table 3.2) were obtained using the equation 2 mentioned in the sub-section 1.3 and the capacitance at 1 kHz. These are lower than expected for the ZrO_x (20-25) [14], [16], [49], however, these are in agreement with reported values for solution

processed zirconium oxide [1], [3], [6]. The ZrO_x films are amorphous and inevitably could contain pores as a consequence of the sol-gel process [6]. This, in turn, produces a film of lower density than a vacuum-deposited crystalline film, and as a result the dielectric constant of the film must be smaller. However, the films still have a much higher dielectric constant value than silicon dioxide (≅ 3.9).

Table 3.2 - Summary of the physical and electrical properties of solution-processed ZrO_x thin films.

Condition	**Solvent**	c (M)	C_i (nF cm^{-2}) **at 1 kHz**	$d_{high-\kappa}$ (nm)	**κ at 1 kHz**	E (MV cm^{-1})	J (A cm^{-2}) **at 1 MV cm^{-1}**
300 °C, 30 min	Ethanol	0.2	438 ± 9	21.9 ± 0.1	10.8 ± 0.2	1.8 ± 0.03	(8.7 ± 0.4) × 10^{-7}
	2-ME	0.2	558 ± 35	13.9 ± 0.2	8.7 ± 0.6	3.4 ± 0.03	(2.2 ± 2.7) × 10^{-8}

Analysing the results, the device annealed at 300 °C with 2-ME exhibited a better performance compared to ethanol, higher average areal capacitance (558 ± 35 nF cm^{-2}) and breakdown electric field (3.4 ± 0.03 MV cm^{-1}). However, ethanol still showed better parameters than some reports of solution-based ZrO_x annealed at 300 °C [1], [18] and has the advantage of being a greener solvent.

3.3.2. Influence of annealing temperature

The annealing process for solution-processed oxide dielectric is a crucial step, since during it, the organic residues are removed and the oxide is formed [1]. To investigate the correlation between the annealing temperature and the electrical performance, the thin films were annealed at various temperatures ranging from 150 °C to 350 °C. To eliminate the need of a high-temperature annealing, the 150 °C thermal annealing assisted by a deep-ultraviolet (DUV) lamp exposure in a N_2 atmosphere was used.

Park et al. have discussed the formation mechanisms of ZrO_x under UV irradiation [21]. One is a relatively fast photolysis of the precursor by the UV irradiation; the other is a slower densification of the thin film due to the oxidation by reactive oxygen species (O*). UV irradiation at UVD (100-200 nm) and UVC (200-275 nm) in atmosphere leads to the production of O_3 and the active oxygen species (O*). The as-spun thin films contain a significant amount of residual organic components, these active species can oxidize the organic ligands and the residual solvent into volatile gases (such as CO_X, H_2O and NO_x) at low temperature. Thus, the photoexcitation of the precursor gives rise to the decomposition of organic groups and the promotion of metal-oxygen (M-O) bonds [3], [54]. The moderate temperature leads to fast film densification because it maximizes M-O-M networks accelerating the diffusion or removal of decomposed impurities and induces the thermal vibration for lowering the activation barrier for condensation [55]. The formation process of the condensed ZrO_x thin film is schematically described in Figure 3.10.

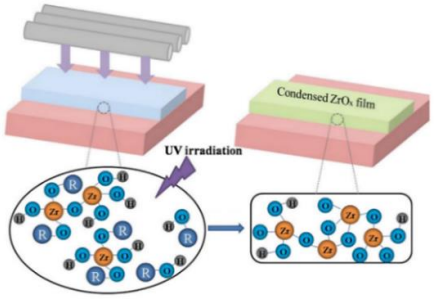

Figure 3.10 - Schematic diagram of the condensation mechanism of ZrO_x precursors by UV irradiation [54].

The Figures 3.11 a) and c) show the areal capacitance of ZrO_x films in the frequency between 1 kHz and 100 kHz for the ethanol absolute and 2-ME, respectively, at different annealing temperatures. The plots demonstrate an apparent trend where the areal capacitance of ZrO_x films increase with increasing annealing temperature. In addition, a weak frequency dispersion of capacitance is observed

for all the conditions, indicating the low defect density, as oxygen vacancies and/or hydroxyl group in thin films [18].

In the $C-V$ (Figure 3.11 b) and d)) curves for the thin films annealed at 150 °C combined with DUV exposure can be observed in the accumulation region that the capacitance has a strong variance with the voltage applied, being the most noticeable effect on thin films that were exposed by the irradiation for less time; 30 min. These results can confirm that when the films are exposed to the irradiation for a longer time than 30 min a higher film quality is obtained. Increasing the annealing temperature up to 250 °C, this variance is no longer observed, which is in agreement with DSC results (sub-section 3.1.1). In addition, the hysteresis width is almost imperceptible for temperatures up to 250 °C, suggesting more defects in the interface or films in ZrO_x-150 °C films.

To evaluate film density and the number of voids in the insulator film, the leakage current density was measured as a function of annealing temperature (insets). The order of magnitude at an electric field of 1 MV cm^{-1} obtained for the different conditions were between 10^{-5} A cm^{-2} and 10^{-8} A cm^{-2} and these do not follow a decrease or increase trend with conditions. Solution-processed gate dielectrics are required to have a low leakage current (< 10^{-5} A cm^{-2}) [2]. The high current ((2.0 ± 2.2) × 10^{-5} A cm^{-2}) exhibited by Ethanol-150 °C + DUV for 1 h can be explained by the presence of defect density; the oxygen vacancies in the high-κ thin films are the main defects density and lead to conduction paths [3]. Another reason is the low thickness of the dielectric films because when aluminium electrodes are deposited by resistive thermal evaporation can cause short circuits, thus becoming a current path through the dielectric, which contributes to high leakage current. On other hand, the low leakage current presented by the other films may originate from the smooth surface, relatively dense film and high oxidation states. The lowest observed value was (5.4 ± 33.4) × 10^{-9} A cm^{-2} for the Ethanol-350 °C film, however, a high relative error is associated (Table 3.5). To a more reliable study of the MIS capacitors electrical properties in function of the annealing temperature, further data and analysis are required.

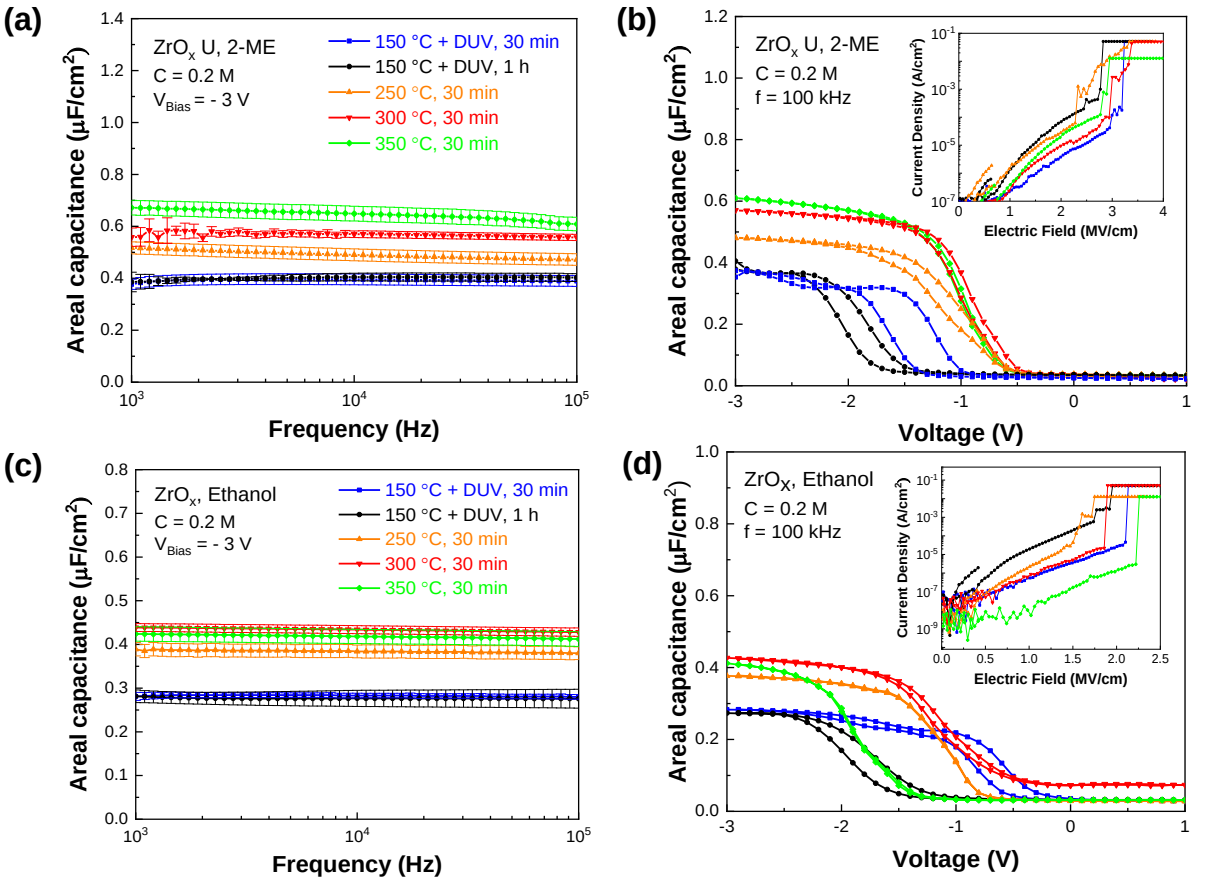

Figure 3.11 – Characteristic curves for 2-ME and ethanol solution-based Al/ZrO_x/p-Si capacitors, respectively, annealed at different temperatures and times: (a, c) Areal capacitance-frequency, (b, d) areal capacitance-voltage to a frequecy of 100 kHz. Inset: Current density-electric field.

Table 3.3 summarizes the physical and electrical properties of the ZrO_x films for different temperatures. As expected, the relative dielectric constants (κ) are relatively low for 150 °C-annealed films when compared with the thin films fabricated at a higher temperature using the same solvent in the precursor solution. This can also be explained by the low atomic density resulting in small electronic and ionic polarizations [1]. Due to the higher dielectric thickness, the ethanol devices exhibit greater dielectric constant for all the conditions. On other hand, analysing the breakdown electric field parameter, the films fabricated with 2-ME exhibited greater values (> 2 MV cm^{-1}).

Table 3.3 - Summary of the physical and electrical properties of solution-processed ZrO_x dielectrics annealed at different temperatures and times (Annex E).

Condition	**Solvent**	***c*** (M)	C_i (nF cm^{-2}) **at 1 kHz**	$d_{high-\kappa}$ (nm)	**κ at 1 kHz**	***E*** (MV cm^{-1})	***J*** (A cm^{-2}) **at 1 MV cm^{-1}**
150 °C + DUV, 30 min	Ethanol	0.2	281 ± 9	25.7 ± 0.1	8.5 ± 0.3	1.9 ± 0.2	(2.2 ± 3.7) × 10^{-7}
	2-ME	0.2	376 ± 19	18.3 ± 0.1	7.7 ± 0.5	2.2 ± 0.6	(2.5 ± 2.3) × 10^{-7}
150 °C + DUV, 60 min	Ethanol	0.2	281 ± 25	24.0 ± 0.1	7.7 ± 0.7	2.3 ± 0.2	(2.0 ± 2.2) × 10^{-5}
	2-ME	0.2	386 ± 37	16.0 ± 0.1	7.1 ± 0.7	2.3 ± 0.5	(1.4 ± 2.7) × 10^{-6}
250 °C, 30 min	Ethanol	0.2	389 ± 15	24.8 ± 0.1	10.8 ± 0.4	1.5 ± 0.2	(2.3 ± 29.9) × 10^{-6}
	2-ME	0.2	517 ± 23	17.0 ± 0.1	9.0 ± 0.4	2.6 ± 0.5	(2.1 ± 23.6) × 10^{-6}
300 °C, 30 min	Ethanol	0.2	438 ± 9	21.9 ± 0.1	10.8 ± 0.2	1.8 ± 0.03	(8.7 ± 0.4) × 10^{-7}
	2-ME	0.2	558 ± 35	13.9 ± 0.2	8.7 ± 0.5	3.4 ± 0.03	(2.2 ± 2.7) × 10^{-8}
350 °C, 30 min	Ethanol	0.2	424 ± 16	21.0 ± 0.1	10.6 ± 0.5	1.6 ± 0.1	(5.4 ± 33.4) × 10^{-9}
	2-ME	0.2	672 ± 28	14.2 ± 0.1	11.0 ± 0.5	2.8 ± 0.1	(3.9 ± 1.1) × 10^{-7}

The parameters obtained demonstrate that low temperatures methods (≤ 350 °C) combined with sol-gel or combustion method could effectively promote the formation of high quality ZrO_x films.

3.3.3. Influence of precursor concentration at low temperature

To study the influence of molar concentration (*c*) in the electrical performance of MIS capacitors, ZrO_x films were prepared with 0.1 M and 0.2 M of zirconium nitrate at different process conditions.

The results for 2-ME solution-based MIS capacitors annealed at 150 °C with DUV irradiation for 1 h are shown in the Figure 3.12.

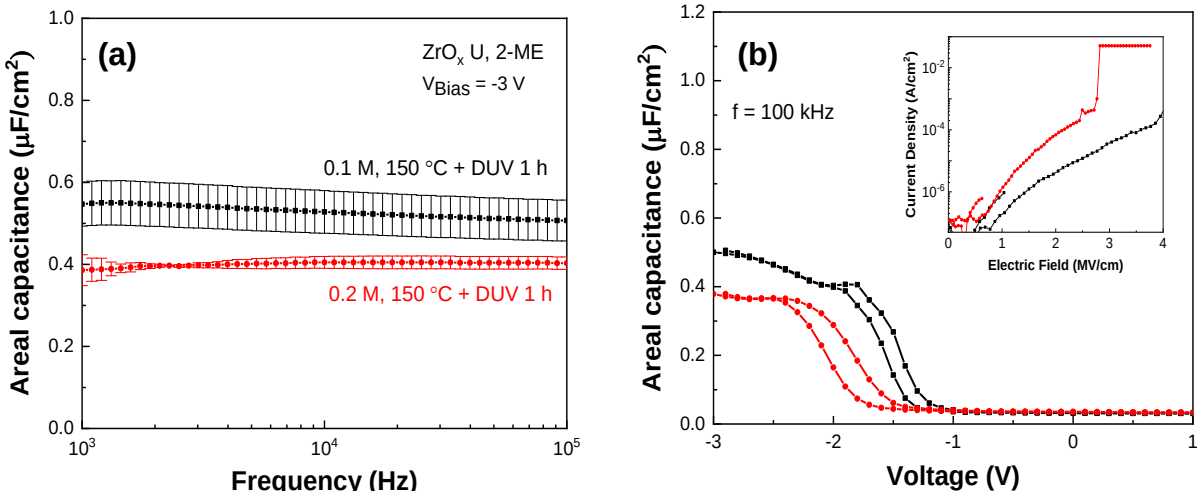

Figure 3.12 – Characteristic curves of 2-ME solution-based Al/ZrO_x/p-Si capacitors for a precursor concentration of 0.2 M and 0.1 M at a annealing temperature of 150 °C + DUV for 1 h: (a) Areal capacitance-frequency and (b) areal capacitance-voltage. Inset : Current density-electric field.

As exhibited in the Figure 3.12, increasing the precursor concentration (c), the dielectric thickness increase (d) and the areal capacitance (C_i) decreases proportionally (equation 2). To understand why the thickness decrease, it is necessary to discuss the film formation process. After the precursor deposition on the substrate, a solution layer is formed containing a large number of ions. This layer has a certain thickness which has a small dependency on the solution properties (viscosity, surface tension and concentration) because in the spin-coating process centrifugal force plays a dominant role. The solution layer has a larger thickness than the final ZrO_x film after post-annealing, and the high concentration precursor results in more ions in the thick layer (Figure 3.13). The Zr and O elements form Zr-O bonds in the solution and films with a certain thickness are formed, which are related to the quantity of Zr ions in the precursor [2].

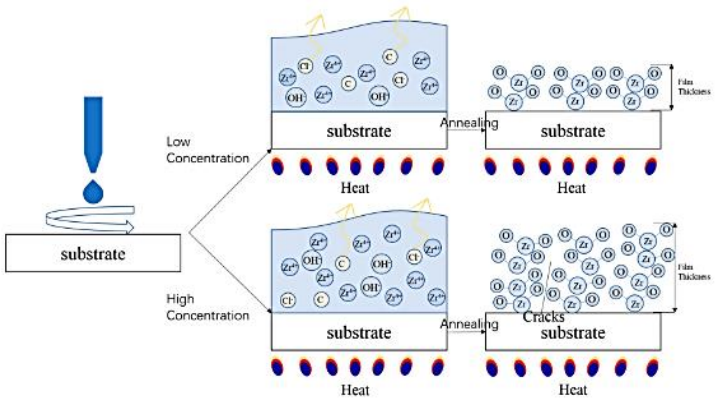

Figure 3.13 – Effect of low and high precursor concentration during the thermal annealing step [2].

As it shows in the inset image in figure 3.12 b), the leakage current density at an electric field of 1 MV cm^{-1} is higher for the 0.2 M film, which indicate more defect density, which also explain the lower value for the breakdown electric field parameter compared with 0.1 M film. The dielectric constant, obtained using the equation 2 and depicted in Table 3.4, is lower for the dielectric with 0.1 M due to the low film thickness.

The same results for other process conditions (Annex F) were obtained, however a lower current density was exhibited for the 2-ME-300 0.2 M dielectric film.

Table 3.4 - Summary of the physical and electrical properties and the relative errors of the devices depicted in Figure 3.12.

Condition	Solvent	c (M)	C_i (nF cm^{-2}) at 1 kHz	$d_{high-\kappa}$ (nm)	K at 1 kHz	E (MV cm^{-1})	J (A cm^{-2}) at 1 MV cm^{-1}
150 °C + DUV, 60 min	2-ME	0.1	547 ± 53	9.7 ± 0.1	5.8 ± 0.6	3.7 ± 0.9	(2.1 ± 0.9) × 10^{-7}
		0.2	386 ± 37	16.0 ± 0.1	7.1 ± 0.7	2.3 ± 0.5	(1.4 ± 2.7) × 10^{-6}

The results for ethanol solution-based MIS capacitors annealed at 150 °C combined with DUV irradiation for 1 h are shown in the Figure 3.14.

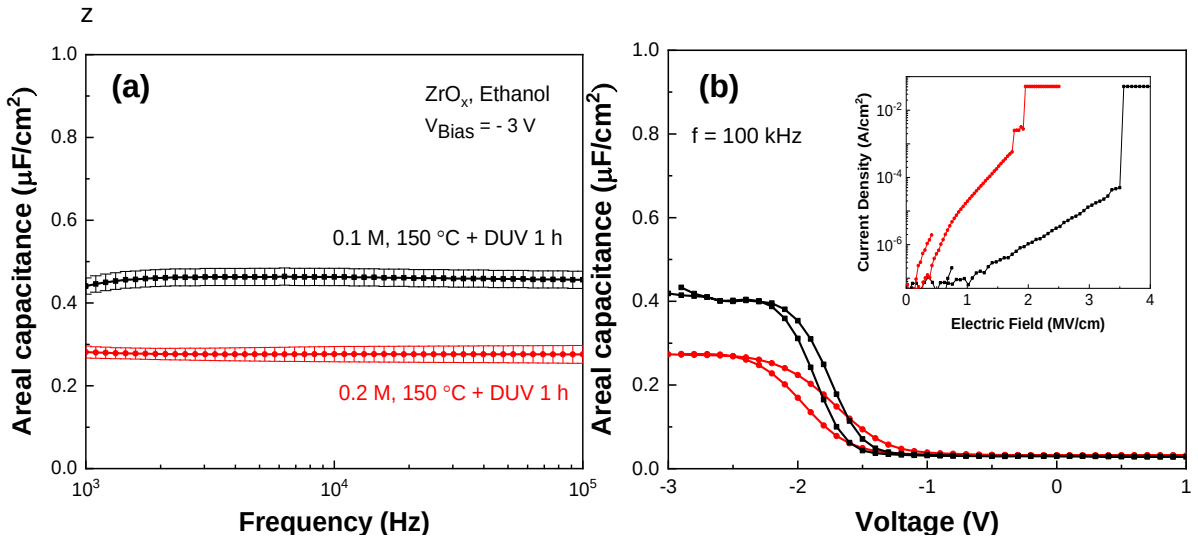

Figure 3.14 - Characteristic curves of ethanol solution-based Al/ZrO$_x$/p-Si capacitors for a precursor concentration of 0.2 M and 0.1 M at a annealing temperature of 150 °C + DUV for 1 h: (a) Areal capacitance-frequency and (b) areal capacitance-voltage. Inset : Current density-electric field.

The same statements can be made for the solution with ethanol as solvent. The areal capacitance decreases with increasing precursor concentration as the reason was explained before (Figure 3.14 a)); the thickness decreases with decreasing precursor concentration; the dielectric constant is lower, and the breakdown electric field is greater for 0.1 M (Table 3.5).

The leakage current density at an electric field of 1 MV cm^{-1} for the different conditions (Table 3.5 and Annex F) does not follow a trend with solution concentration, being the Ethanol-350 0.2 M film with the lowest parameter value.

Table 3.5 - Summary of the physical and electrical properties and the relative errors of the devices depicted in Figure 3.14.

Condition	Solvent	c (M)	C_i (nF cm^{-2}) at 1 kHz	$d_{high-\kappa}$ (nm)	K at 1 kHz	E (MV cm^{-1})	J (A cm^{-2}) at 1 MV cm^{-1}
150 °C + DUV, 60 min	Ethanol	0.1	441 ± 4	13.3 ± 0.1	6.7 ± 0.1	3.5 ± 0.1	(2.1 ± 0.9) × 10^{-7}
		0.2	281 ± 25	24.0 ± 0.1	7.7 ± 0.7	2.3 ± 0.2	(2.0 ± 2.2) × 10^{-5}

The 0.1 M capacitors exhibited a better electrical performance for both solutions but the measurement process using the probe station tips was challenging due to their very low thickness. In addition, in the $C-V$ graphs for all the 0.1 M films, a higher capacitance variation with frequency between 1 kHz and 100 kHz was observed.

Due to the greater thickness present by 0.2 M films that allows their application in flexible capacitors, they were intensively studied in this work and it were chosen to be applied as gate insulators in TFTs as proof of concept (Section 3.4).

3.3.4. Influence of solution aging

ZrO_X based-solutions were produced and spin-coated on silicon wafers after 1 month, to study the solution stability from MIS capacitors electrical performance. This section is divided by solutions with different solvents. The results for the 2-ME solution-based MIS capacitors annealed at 300 °C for 30 min are shown in the Figure 3.15.

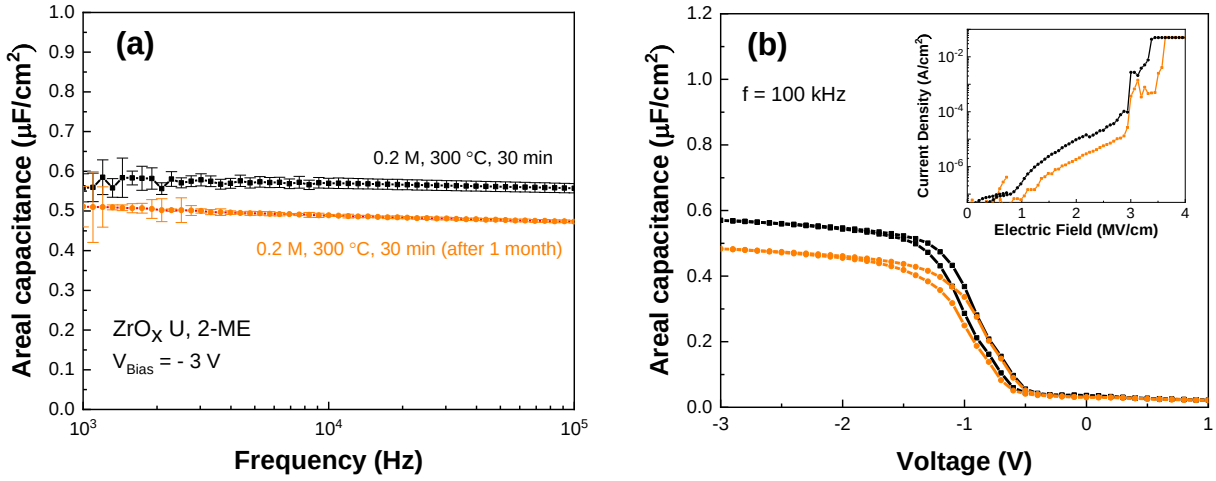

Figure 3.15 – (a) Areal capacitance-frequency, (b) areal capacitance-voltage and currenty density-electric field curves in the inset for 2-ME solution-based Al/ZrO_X/p-Si capacitors produced from different solutions time: i) solution used 1 month after being produced (orange graph), ii) solution used in the same day that was produced (black graph).

Comparing the both plots differentiated by the solution shelf time, small variations can be noticed. According to the Table 3.6, a small variation of ≅ 8 % is obtained for the capacitance values at 1 kHz, ≅ 7.5 % for the dielectric constant and only ≅ 3.5 % for the breakdown electric field values. Thus, it can be concluded that variations exist between the capacitors but are not very high. In addition, the film with the solution used 1 moth after exhibited a lower leakage current of $(8.6 \pm 2.9) \times 10^{-8}$ A cm^{-2} at 1 MV cm^{-1}, one order of magnitude lower than the 1-day solution.

Table 3.6 - Summary of the physical and electrical properties and the relative errors for the devices depicted in Figure 3.15.

Condition	Solvent	c (M)	Solution time	C_i (nF cm^{-2}) at 1 kHz	κ at 1 kHz	E (MV cm^{-1})	J (A cm^{-2}) at 1 MV cm^{-1}
300 °C, 30 min	2-ME	0.2	1 moth	511 ± 6	8.0 ± 0.1	3.5 ± 0.1	$(8.6 \pm 2.9) \times 10^{-8}$
		0.2	1 day	558 ± 35	8.7 ± 0.5	3.4 ± 0.03	$(3.7 \pm 2.7) \times 10^{-7}$

The ethanol solution-based MIS capacitor annealed at 300 °C for 30 min are shown in the Figure 3.16.

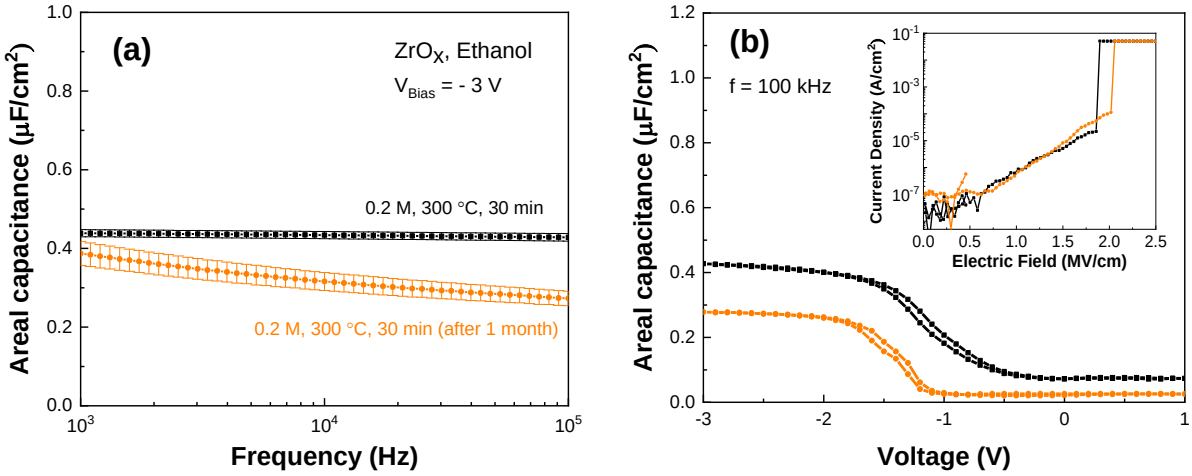

Figure 3.16 - (a) Areal capacitance-frequency, (b) areal capacitance-voltage and currenty density-electric field curves in the inset for ethanol solution-based Al/ZrO_x/p-Si capacitors produced from different solutions time: i) solution used 1 month after being produced (orange graph), ii) solution used in the same day that was produced (black graph).

In the $C-f$ graphs, a strong capacitance variance with the frequency (≅ 27 %) between 1 kHz and 100 kHz is observed in the 1-month solution, which indicates a film with high defect density may originate from an unstable solution. As depicted in the Table 3.7, a variation of ≅ 11.6 % is obtained for the capacitance values at 1 kHz, ≅ 9.7 % for the dielectric constant and ≅ 9.4 % for the breakdown electric field values.

Table 3.7 - Summary of the physical and electrical properties and the relative errors of the devices depicted in the Figure 3.16.

Condition	**Solvent**	***c*** (M)	**Solution time**	C_i **(nF cm^{-2}) at 1 kHz**	**K at 1 kHz**	***E*** (MV cm^{-1})	***J*** (A cm^{-2}) **at 0.5 MV m^{-1}**
300 °C, 30 min	Ethanol	0.2	1 moth	387 ± 30	9.7 ± 0.7	2.0 ± 0.02	(7.1 ± 2.0) × 10^{-7}
		0.2	1 day	438 ± 9	10.8 ± 0.2	1.8 ± 0.03	(1.1 ± 0.4) × 10^{-6}

Taking into account the results obtained it was concluded that the solutions with ethanol and 2-ME as solvents suffer alterations over time affecting negatively the electrical performance of the devices, however, the capacitance variance with frequency was much lower for the 2-ME solution-based capacitors than ethanol solution-based capacitors. To obtain consistent results new solutions were produced every week.

3.3.5. Flexible MIM capacitors

After the successful fabrication of high-quality amorphous ZrO_x films by the low temperature of 150 °C combined with DUV treatment for 1 h, the application of solution-processed ZrO_x films on flexible substrates was investigated. Metal-insulator-metal (MIM) capacitors Au/ZrO_x/Al structured on Kapton were fabricated. This polyimide film was chosen as substrate due to it high thermal stability (up to 300 °C) and high chemical resistance to acetone and isopropyl alcohol [56].

To analyse the surface morphology of the devices, some imagens were taken with the optical microscope. Figure 3.17 a) shows the surface morphology of a MIM flexible device and the Figure 3.17 b) a MIS device structured on Si, both with the same annealing step. It clearly shows the difference between the substrates; the left device exhibits high surface roughness and the right one a smooth

surface. AFM was also used to obtain the surface roughness (Annex G) of the polyimide substrate and a value of ≅ 3.4 nm was obtained.

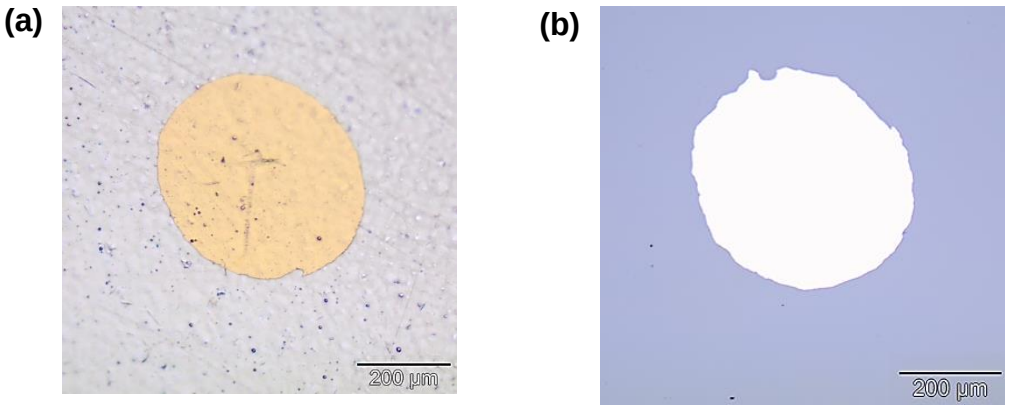

Figure 3.17 - Surface morphology of solution-based capacitors produced with 0.2 M zirconium nitrate precursor using urea as fuel in 2-ME: (a) MIM structured capacitor with 2 dielectrics layers deposited on an polyimide film and (b) MIS structured capacitor with 1 dielectric layer deposited on a silicon wafer.

The capacitors produced with 2 dielectric layers and a solution of 0.2 M zirconium nitrate precursor using urea as fuel in 2-ME were the only ones that showed desirable characteristics. The 2 dielectric layers instead helped to overcome possible problems caused by the high surface roughness substrate. Figures 3.18 a) and b) show the electrical performance of this flexible device. The inset of the Figure 3.18 a) shows the capacitor image under bending indicating its flexibility.

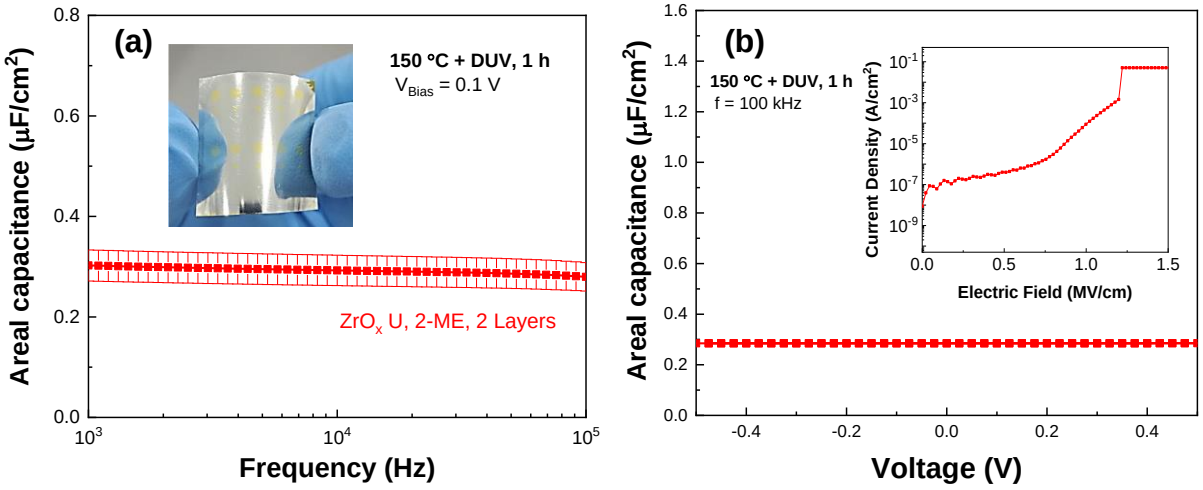

Figure 3.18 – Characteristic curves of MIM capacitors deposited on flexible substrate: (a) Areal capacitance-frequency and a image of the devices in the inset, (b) areal capacitance-voltage and current density-electric field in the inset.

In the $C - f$ graph (Figure 3.18 a)) a weak capacitance variation with frequency between 1 kHz and 100 kHz is observed. The capacitance does not change with the applied voltage in metal-insulator-metal (MIM) capacitors, as was explained in the section 1.3 (Figure 3.18 b)). The characteristic parameters of the device can be seen in Table 3.8. The device shows a leakage current of (4.7 ± 4.7) × 10^{-7} A cm^{-2} at 0.5 MV cm^{-1} and (1.2 ± 2.3) × 10^{-4} A cm^{-2} at 1 MV cm^{-1}. The breakdown electric field obtained was 1.0 ± 0.2 MV cm^{-1}. The high leakage current at 1 MV cm^{-1} and the low breakdown electric field are due to the high roughness of the flexible substrate.

Table 3.8 - Summary of the physical and electrical properties of the devices depicted in the Figure 3.18.

Condition	Solvent	c (M)	C_i (nF cm^{-2}) at 1 kHz	$d_{high-\kappa}$ (nm)	κ at 1 kHz	E (MV cm^{-1})	J (A cm^{-2}) at 0.5 MV cm^{-1}
150 °C + DUV, 60 min (2 Layers)	2-ME	0.2	302 ± 31	33.8 ± 0.1	11 ± 1	1.0 ± 0.2	(4.7 ± 4.7) × 10^{-7}

Although performance is not as good as for devices on Si substrates, the results are promising, and process optimization should lead to further improvement in flexible electronic devices.

3.4. Electrical Characterization of solution-based TFTs

3.4.1. Proof of concept

The best precursor solution, using zirconium nitrate as precursor (0.2 M) and urea (U) as fuel in 2-ME, was used to deposit optimized ZrO_x dielectric films to be applied in solution-based In_2O_3 TFTs. Considering that the In_2O_3 semiconductor layer needs a minimum temperature of 200 °C to achieve a good film densification, the different TFT layers were annealed at the same temperature or higher (200 °C + FUV irradiation and 300 °C for 30 min).

The MIS capacitor annealed at 200 °C combined with FUV exhibited an average capacitance of 460 ± 20 nF cm^{-2}, a dielectric constant of 7.8 ± 0.3 and a breakdown electric field of 3.2 ± 0.5 MV cm^{-1} (Annex H). The capacitor annealed at 300 °C showed an average capacitance of 558 ± 35 nF cm^{-2}, a dielectric constant of 8.7 ± 0.5 and a breakdown electric field of 3.4 ± 0.03 MV cm^{-2} (Sub-section 3.3.1).

Figure 3.19 exhibits the In_2O_3 / ZrO_x TFTs transfer curves ($I_D - V_G$) with an applied gate voltage between -1 V and 2 V and drain voltage (V_{DS}) of 2 V. It shows that the drain current (I_D) is lower for the TFT-200 °C (Figure 3.19 a)), what was expected due to the lower capacitance exhibited by the dielectric film. However, it still shows a better modulation than TFT-300 °C (Figure 3.19 b)) and therefore a higher On/Off current ratio.

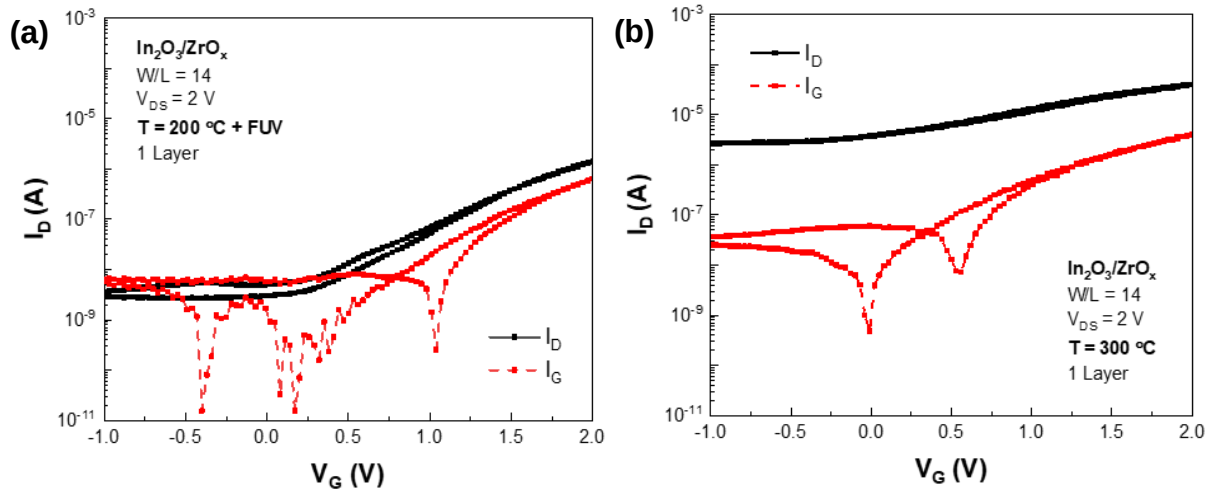

Figure 3.19 - Transfer characteristics of In_2O_3/ZrO_x TFTs with a *W/L* of 14 (a) annealed at 200 °C combining FUV irradiation for 30 min and (b) annealed at 300 °C for 30 min.

The characteristic parameters for both TFTs are depicted in the Table below. The TFT annealed at lower temperature exhibited higher I_{ON}/I_{OFF} ratio (as expected by curve modulation) and lower

subthreshold swing (SS). The 300 °C-annealed TFT showed a higher field effect mobility of 2.5 $cm^2\ V^{-1}\ s^{-1}$.

Table 3.9 -Summary of the eletrical properties of solution-based In_2O_3/ZrO_x TFTs depicted in Figure 3.19.

Layers Condition	**Dielectric Capacitance** (nF cm^{-2}) **at 1 kHz**	I_{ON}/I_{OFF}	SS (V $decade^{-1}$)	μ_{FE} ($cm^2\ V^{-1}\ s^{-1}$)
200 °C + FUV, 30 min	460 ± 20	5×10^2	0.5	0.2
300 °C, 30 min	558 ± 35	1.5×10^1	1.5	2.5

A successful application of the ZrO_x films as gate insulators in TFTs with a low operation voltage was demonstrated, however further work needs to be done to improve the TFTs performance.

4. Conclusion and Future Perspectives

This dissertation demonstrates the sucessful production of high-quality ZrO_x films by sol-gel and combustion method using different annealing temperatures, combined or not with process engineering (UV post-treatments), and times, different types of solvents (2-methoxyethanol and the environmental friendly ethanol) and precursor concentrations.

The solutions produced by combustion method with non-stoichiometric molar proportion were investigated and it was concluded that the fuel rich solutions showed similar behaviour with temperature variation when compared with the balanced stoichiometry solution. The structural analysis of the ZrO_2 powder obtained at 350 °C showed a polycrystalline phase. On other hand, the thin films annealed at 350 °C are amorphous. These results demonstrate that the quantity of precursor solution is fundamental to define the zirconia phase and that the thin films have a smooth surface enhancing the applicability as gate insulators.

Transmittance spectra showed the thin films applicability in transparent electronic, it verified that all films in the visible region exhibited transparency over 80 %. It was found by chemical characterization that the annealing step is essential in solution-processed films because it can effectively reduce the residual organic components in the gel films and promote the condensation of them. The ethanol solution-based ZrO_x films showed higher thickness for all process conditions which may originate from higher solution viscosity. On other hand, 2-ME solution-based ZrO_x films exhibited higher band gap, demonstrating the band gap dependence with film thickness attributed to the quantum confinement effect. It was also confirmed that the thickness can be controlled by number of layers and molar concentration of ZrO_x precursor solution.

To evaluate the electrical characteristics of 0.1 M and 0.2 M thin films, a uniform and reproducible study of capacitors devices was performed where more than 6 devices with an area of 0.2 mm^2 showed a good performance and an average of them was obtained. In the $C-f$ plots, the 0.2 M capacitors with both solutions showed small variability of capacitance with frequency and small width hysteresis indicating low defect density The devices performance demonstrated that low temperatures methods (≤ 350 °C) combined with sol-gel or combustion method can effectively promote the formation of high quality ZrO_x films. Even through the dielectric constants (κ) values at 1 kHz were lower than expected, they are in agreement with reported values for solution processed zirconium oxide. The low leakage current density values (< 10^{-5} A cm^{-2}) demonstrated the possibility for thin films application as gate insulators in solution-based TFTs.

Comparing the capacitors fabricated with different solutions, the 0.2 M 2-ME solution-based capacitors showed better performance. The capacitors annealed at 300 °C exhibited an average leakage current density of (2.2 ± 2.7) × 10^{-8} at 1 MV cm^{-1}, a large average breakdown electric field of 3.4 ± 0.03 MV cm^{-1} and an areal capacitance in the accumulation region of 558 ± 35 nF cm^{-2} . However, the ethanol has the advantage of being a greener solvent and the 0.2 M capacitors still showed better performance than some reports of solution-based ZrO_x annealed at 300 °C, as an average constant dielectric of 10.8 ± 0.2 and an areal capacitance of 438 ± 9 nF cm^{-2}. The devices with a precursor molar concentration of 0.1 M exhibited better electrical properties, however, an unstable behaviour was noticed during the measurements generated due to the lower thickness of the films when compared with 0.2 M films. In addition, the greater thickness exhibited by 0.2 M films allow the fabrication of capacitors on flexible substrates.

Studying the influence of solution aging in the electrical performance of devices, it was noticed that both solutions suffer changes over time affecting negatively their performance, with the ethanol solution-based capacitors showing a higher capacitance variance with frequency of ≅ 27 %. The 2-ME solution-based capacitors showed a small variation of ≅ 7 %.

The solution-based ZrOx dielectrics presented in this work show electrical properties equivalent to or even in some cases overcome the published results being relevant for the state-of-the-art (Annex I).

All the thin films were annealed at low temperature and can be applied in flexible substrates as seen for 2-ME solution-based capacitors deposited on a Kapton substrate using a thermal annealing of 150 °C combined with DUV irradiation. These showed an average dielectric constant of 11 ± 1 and a

low leakage current of (4.7 ± 4.7) × 10^{-7} A cm^{-2} at 0.5 MV cm^{-1}. However, the performance is not as good as for devices in Si substrates due to the high roughness of the Kapton substrate (≅ 3.4 nm), but the results are promising, and process optimization should lead to further improvement.

The solution-based In_2O_3/ZrO_x TFTs where FUV irradiation followed thermal annealing at 200 °C was used exhibited a higher On/Off current ratio and subthreshold swing (SS) than the TFTs annealed at 300 °C. On other hand, these last showed a higher field effect mobility.

To conclude, this work clearly shows that a low temperature treatment combined with a solution process method is suitable to achieve high quality amorphous ZrO_x films, so that it will be promising for future low cost, flexible, low power comsuption device applications. However, the study and optimization of ZrO_x dielectrics must continue to achieve even better results. There are many steps that sould be do to continue this work:

- Study the dieletric performance with multilayers;
- Study the capacitors stability over time;
- Try to produce other solutions with green solvents, as supercritical CO_2 and ionic liquids (ILs);
- Evaluate the devices performance with alternative flexible substrates, as PEN and PET polymer substrates;
- Produce flexible TFTs with the optimized ZrO_x thin films;
- Use printing techonologies, as screen printing and inkjet printing, to deposite the device electrodes;
- Apply the solution-based ZrO_x films as surface passivation layers in solar cells.

5. References

[1] Y. Gong, K. Zhao, H. He, *et al.*, “Solution processable high quality ZrO2 dielectric films for low operation voltage and flexible organic thin film transistor applications,” *J. Phys. D. Appl. Phys.*, vol. 51, no. 11, 2018.

[2] W. Cai, Z. Zhu, J. Wei, *et al.*, “A simple method for high-performance, solution-processed, amorphous ZrO2 gate insulator TFT with a high concentration precursor,” *Materials (Basel).*, vol. 10, no. 8, 2017.

[3] G. X. Liu, A. Liu, Y. Meng, F. K. Shan, B. C. Shin, W. J. Lee, and C. R. Cho, “Annealing Dependence of Solution-Processed Ultra-Thin ZrOx Films for Gate Dielectric Applications,” *J. Nanosci. Nanotechnol.*, vol. 15, no. 3, pp. 2185–2191, 2014.

[4] S. Park, C. H. Kim, W. J. Lee, S. Sung, and M. H. Yoon, “Sol-gel metal oxide dielectrics for all-solution-processed electronics,” *Mater. Sci. Eng. R Reports*, vol. 114, pp. 1–22, 2017.

[5] J. Cho, P. Choi, N. Lee, S. Kim, and B. Choi, “Dielectric Properties of Solution-Processed ZrO2 for Thin-Film Transistors,” *J. Nanosci. Nanotechnol.*, vol. 16, no. 10, pp. 10380–10384, 2016.

[6] J. B. Seon, N. K. Cho, G. Yoo, Y. S. Kim, and K. Char, “Solution-processed amorphous ZrO2 gate dielectric films synthesized by a non-hydrolytic sol-gel route,” *RSC Adv.*, vol. 8, no. 68, pp. 39115–39119, 2018.

[7] K. Kanayama, K. Nagashio, T. Nishimura, and A. Toriumi, “Large Fermi energy modulation in graphene transistors with high-pressure O2-annealed Y2O3 topgate insulators,” *Appl. Phys. Lett.*, vol. 104, no. 8, pp. 10–15, 2014.

[8] Y. Hu, C. Wang, H. Dong, R. M. Wallace, K. Cho, W. H. Wang, and W. Wang, “Origin of Indium Diffusion in High-k Oxide HfO2,” *ACS Appl. Mater. Interfaces*, vol. 8, no. 11, pp. 7595–7600, 2016.

[9] B. Y. Chou, C. S. Lee, C. L. Yang, W. C. Hsu, H. Y. Liu, M. H. Chiang, W. C. Sun, S. Y. Wei, and S. M. Yu, “TiO2-dielectric AlGaN/GaN/Si metal-oxide-semiconductor high electron mobility transistors by using nonvacuum ultrasonic spray pyrolysis deposition,” *IEEE Electron Device Lett.*, vol. 35, no. 11, pp. 1091–1093, 2014.

[10] S. Gieraltowska, L. Wachnicki, B. S. Witkowski, E. Guziewicz, and M. Godlewski, “Thin films of high-k oxides and ZnO for transparent electronic devices,” *Chem. Vap. Depos.*, vol. 19, no. 4–6, pp. 213–220, 2013.

[11] P. Gogoi, R. Saikia, D. Saikia, R. P. Dutta, and S. Changmai, “ZnO TFTs prepared by chemical bath deposition technique with high-k La2O3 gate dielectric annealed in ambient atmosphere,” *Phys. Status Solidi Appl. Mater. Sci.*, vol. 212, no. 4, pp. 826–830, 2015.

[12] C. G. Lee and A. Dodabalapur, “Solution-processed high-k dielectric, ZrO2, and integration in thin-film transistors,” *J. Electron. Mater.*, vol. 41, no. 5, pp. 895–898, 2012.

[13] G. D. Wilk, R. M. Wallace, and J. M. Anthony, “High-κ gate dielectrics: Current status and materials properties considerations,” *J. Appl. Phys.*, vol. 89, no. 10, pp. 5243–5275, 2001.

[14] D. Q. Xiao, G. He, J. G. Lv, *et al.*, “Interfacial modulation and electrical properties improvement of solution-processed ZrO2 gate dielectrics upon Gd incorporation,” *J. Alloys Compd.*, vol. 699, pp. 415–420, 2017.

[15] L. Xifeng, X. Enlong, and Z. Jianhua, “Low-temperature solution-processed zirconium oxide gate insulators for thin-film transistors,” *IEEE Trans. Electron Devices*, vol. 60, no. 10, pp. 3413–3416, 2013.

[16] J. P. Chang and Y. S. Lin, “Dielectric property and conduction mechanism of ultrathin zirconium oxide films,” *Appl. Phys. Lett.*, vol. 79, no. 22, pp. 3666–3668, 2001.

[17] H. Wang, W. Xu, S. Zhou, F. Xie, Y. Xiao, L. Ye, J. Chen, and J. Xu, “Oxygen plasma assisted high performance solution-processed Al2Ox gate insulator for combustion-processed InGaZnOx thin film transistors,” *J. Appl. Phys.*, vol. 117, no. 3, 2015.

[18] L. Zhu, G. He, J. Lv, E. Fortunato, and R. Martins, “Fully solution-induced high performance indium oxide thin film transistors with ZrOx high-k gate dielectrics,” *RSC Adv.*, vol. 8, no. 30, pp. 16788–16799, 2018.

[19] E. Carlos, R. Branquinho, A. Kiazadeh, J. Martins, P. Barquinha, R. Martins, and E. Fortunato, “Boosting Electrical Performance of High-κ Nanomultilayer Dielectrics and Electronic Devices by Combining Solution Combustion Synthesis and UV Irradiation,” *ACS Appl. Mater. Interfaces*, vol. 9, no. 46, pp. 40428–40437, 2017.

[20] A. Liu, G. X. Liu, H. H. Zhu, F. Xu, E. Fortunato, R. Martins, and F. K. Shan, “Fully Solution In2O3 TFT Using ZrOx Dielectric,” *ACS Appl. Mater. Interfaces*, vol. 6, no. 20, pp. 17364–17369, 2014.

[21] Y. M. Park, J. Daniel, M. Heeney, and A. Salleo, “Room-temperature fabrication of ultrathin oxide gate dielectrics for low-voltage operation of organic field-effect transistors,” *Adv. Mater.*, vol. 23, no. 8, pp. 971–974, 2011.

[22] K. N. Woods, E. C. Waddington, C. A. Crump, *et al.*, “Tunable high-κ Zr x Al 1−x O y thin film dielectrics from all-inorganic aqueous precursor solutions,” *RSC Adv.*, vol. 7, no. 62, pp. 39147–39152, 2017.

[23] Y. Meng, G. Liu, A. Liu, H. Song, Y. Hou, B. Shin, and F. Shan, “Low-Temperature Fabrication of High Performance Indium Oxide Thin Film Transistors,” *RSC Adv.*, vol. 6, no. 207890, pp. 22469–22475, 2013.

[24] K. Häckl and W. Kunz, “Some aspects of green solvents,” *Comptes Rendus Chim.*, vol. 21, no. 6, pp. 572–580, 2018.

[25] E. V. Capela, J. A. P. Coutinho, and M. G. Freire, “Application of Ionic Liquids in Separation and Fractionation Processes,” *Encycl. Sustain. Sci. Technol.*, pp. 1–29, 2018.

[26] T. Welton, “Solvents and sustainable chemistry Subject Areas,” *R. Soc. Publ.*, vol. 471, pp. 1–26, 2015.

[27] C. Capello, U. Fischer, and K. Hungerbühler, “What is a green solvent? A comprehensive framework for the environmental assessment of solvents,” *Green Chem.*, vol. 9, no. 9, pp. 927–934, 2007.

[28] J. Płotka-Wasylka, M. Rutkowska, K. Owczarek, M. Tobiszewski, and J. Namieśnik, “Extraction with environmentally friendly solvents,” *TrAC - Trends in Analytical Chemistry*, vol. 91. pp. 12–25, 2017.

[29] G. X. Liu, A. Liu, F. K. Shan, Y. Meng, B. C. Shin, E. Fortunato, and R. Martins, “High-performance fully amorphous bilayer metal-oxide thin film transistors using ultra-thin solution-processed ZrOx dielectric,” *Appl. Phys. Lett.*, vol. 105, no. 11, pp. 1–6, 2014.

[30] X. Dong, G. Xia, Q. Zhang, L. Li, H. Gong, J. Bi, and S. Wang, “Room-temperature UV-ozone assisted solution process for zirconium oxide films with high dielectric properties,” *Ceram. Int.*, vol. 43, no. 17, pp. 15205–15213, 2017.

[31] H. Shaaban, A. Mostafa, W. Alhajri, L. Almubarak, and K. AlKhalifah, “Development and validation of an eco-friendly SPE-HPLC-MS method for simultaneous determination of selected parabens and bisphenol A in personal care products: Evaluation of the greenness profile of the developed method,” *J. Liq. Chromatogr. Relat. Technol.*, vol. 41, no. 10, pp. 621–628, 2018.

[32] R. D. Deshpande, *Capacitors: Technology and Trends*. Tata McGraw Hill Education, 2012.

[33] C. Platt and F. Jansson, *Encyclopedia of Electronic Components Volume 1: Resistors,*

Capacitors, Inductors, Switches, Encoders, Relays, Transistors, Vol. 1. MAKERMEDIA, 2016.

[34] M. Rudan, *Physics of Semiconductor Devices*, 3rd ed. Hoboken, NJ, USA: John Wiley & Sons, Inc., 2015.

[35] E. Y. Wu, R. P. Vollertsen, and J. Suñé, "Dielectric Characterization and Reliability Methodology," *Reliab. Wearout Mech. Adv. C. Technol.*, pp. 71–208, 2009.

[36] E. H. Nicollian and J. R. Brews, *MOS (Metal Oxide Semiconductor) Physics and Technology*. New Jersey: Wiley-Interscience, 2002.

[37] K. Lehovec and Shi-Tron Lin, "Analysis of C-V data in the accumulation regime of MIS structures," *Solid State Electron.*, vol. 19, no. 12, pp. 993–996, 1976.

[38] E. Abreu and A. Carlos, "Oxide transistors produced by solution : influence of annealing parameters on properties of the insulating," pp. 1–17, 2015.

[39] N. C. S. Selvam, A. Manikandan, L. J. Kennedy, and J. J. Vijaya, "Comparative investigation of zirconium oxide (ZrO2) nano and microstructures for structural, optical and photocatalytic properties," *J. Colloid Interface Sci.*, vol. 389, no. 1, pp. 91–98, 2013.

[40] S. N. Basahel, T. T. Ali, M. Mokhtar, and K. Narasimharao, "Influence of crystal structure of nanosized ZrO2 on photocatalytic degradation of methyl orange," *Nanoscale Res. Lett.*, vol. 10, no. 1, 2015.

[41] T. J. Webster and M. Sh-eldin, "Physicochemical properties, cytotoxicity, and antimicrobial activity of sulphated zirconia nanoparticles," pp. 765–774, 2015.

[42] H. Lee, X. Zhang, J. W. Kim, E. J. Kim, and J. Park, "Investigation of the electrical characteristics of bilayer ZnO/In2O3 thin-film transistors fabricated by solution processing," *Materials (Basel).*, vol. 11, no. 11, 2018.

[43] V. G. Deshmane and Y. G. Adewuyi, "Synthesis of thermally stable, high surface area, nanocrystalline mesoporous tetragonal zirconium dioxide (ZrO2): Effects of different process parameters," *Microporous Mesoporous Mater.*, vol. 148, no. 1, pp. 88–100, 2012.

[44] A. Ortiz and J. C. Alonso, "Spray Deposition and Characterization of Zirconium-Oxide Thin Films," vol. 34, no. 2, pp. 1–6, 2005.

[45] Y. Adraider, Y. X. Pang, F. Nabhani, S. N. Hodgson, M. C. Sharp, and A. Al-Waidh, "Fabrication of zirconium oxide coatings on stainless steel by a combined laser/sol-gel technique," *Ceram. Int.*, vol. 39, no. 8, pp. 9665–9670, 2013.

[46] F. Heshmatpour and R. B. Aghakhanpour, "Synthesis and characterization of nanocrystalline zirconia powder by simple sol-gel method with glucose and fructose as organic additives," *Powder Technol.*, vol. 205, no. 1–3, pp. 193–200, 2011.

[47] J. J. Yu, J. Y. Zhang, and I. W. Boyd, "Formation of stable zirconium oxide on silicon by photo-assisted sol-gel processing," in *Applied Surface Science*, 2002, vol. 186, no. 1–4, pp. 190–194.

[48] G. Falcony, M. Reyna-García, M. Aguilar-fruits, and C. Falcony, "Electrical, optical and structural characterization of high-k dielectric ZrO2 thin films deposited by the pyrosol technique," *J. Mater. Sci. Mater. Electron.*, vol. 15, no. 7, pp. 439–446, 2004.

[49] P. Jain and P. Arun, "Influence of grain size on the band-gap of annealed SnS thin films," *Thin Solid Films*, vol. 548, pp. 241–246, 2013.

[50] E. S. M. Goh, T. P. Chen, C. Q. Sun, and Y. C. Liu, "Thickness effect on the band gap and optical properties of germanium thin films," *J. Appl. Phys.*, vol. 107, no. 2, pp. 1–5, 2010.

[51] K. Joy, L. V. Maneeshya, J. K. Thomas, and P. V. Thomas, "Effect of sol concentration on the structural, morphological, optical and photoluminescence properties of zirconia thin films," *Thin Solid Films*, vol. 520, no. 7, pp. 2683–2688, 2012.

[52] E. R. Adlard, “Francesca M. Kerton and Ray Marriott: Alternative Solvents for Green Chemistry, 2nd Edition,” *Chromatographia*, vol. 77, no. 17–18, pp. 1249–1250, Sep. 2014.

[53] J. Robertson, “High dielectric constant gate oxides for metal oxide Si transistors,” *Reports Prog. Phys.*, vol. 69, no. 2, pp. 327–396, 2006.

[54] A. Liu, G. X. Liu, F. K. Shan, H. H. Zhu, S. Xu, J. Q. Liu, B. C. Shin, and W. J. Lee, “Room-temperature fabrication of ultra-thin ZrOx dielectric for high-performance InTiZnO thin-film transistors,” *Curr. Appl. Phys.*, vol. 14, no. SUPPL. 1, pp. 39–43, 2014.

[55] Y. J. Jeong, D. J. Yun, S. Nam, E. H. Suh, C. E. Park, T. K. An, and J. Jang, “Photo-patternable high-k ZrOx dielectrics prepared using zirconium acrylate for low-voltage-operating organic complementary inverters,” *Org. Electron. physics, Mater. Appl.*, vol. 33, pp. 40–47, 2016.

[56] P. Taptimthong, J. Rittinger, M. C. Wurz, and L. Rissing, “Flexible magnetic writing / reading system : Polyimide film as flexible substrate,” *Procedia Technol.*, vol. 15, pp. 230–237, 2014.

[57] R. Branquinho, A. Santa, E. Carlos, D. Salgueiro, P. Barquinha, R. Martins, and E. Fortunato, “Solution Combustion Synthesis: Applications in Oxide Electronics,” in *Developments in Combustion Technology*, InTech, 2016.

[58] S. R. Jain, K. C. Adiga, and V. R. Pai Verneker, “A new approach to thermochemical calculations of condensed fuel-oxidizer mixtures,” *Combust. Flame*, vol. 40, no. C, pp. 71–79, 1981.

[59] S. L. González-Cortés and F. E. Imbert, “Fundamentals, properties and applications of solid catalysts prepared by solution combustion synthesis (SCS),” *Applied Catalysis A: General*, vol. 452. pp. 117–131, 2013.

6. Annexes

6.1. Annex A

The combustion method uses the advantage of the propellant chemistry in making the redox mixtures, in which the metal precursor (Zirconium oxide nonahydrate) acts as an oxidizing reactant and fuel (Urea) as a reducing reactant [39]. The solvent used in the overall reaction was the 2-Methoxyethanol ($C_3H_8O_2$). The solvent can play more than one role in systems with more than one metallic cation, as ZTO solutions. In the case of systems with only one metallic cation, as the case of aluminum oxide dielectric, using different solvents was noticed no variation in the exothermic peak [57]. Thus, the solution is not affected by the solvent in this case.

Table 6.1 - Reactions of oxidation, reduction and overall reaction combined by this two.

Reduction Reaction	
Zirconium oxide nonahydrate	$ZrO(NO_3)_2 \cdot xH_2O \xrightarrow[\mathbf{T_b = 124\ °C}]{\mathbf{C_3H_8O_2}} ZrO_x + H_2O + N_2 + O_2$
Oxidation Reaction	
Urea	$CO(NH_2)_2 + \left(\frac{3}{2}\right) O_2 \xrightarrow[\mathbf{T_b = 124\ °C}]{\mathbf{C_3H_8O_2}} 2H_2O + CO_2 + N_2$
Overall Reaction	
Zirconium oxide nonahydrate + Urea	$ZrO(NO_3)_2 + CO(NH_2)_2 \xrightarrow[\mathbf{T_b = 124\ °C}]{\mathbf{C_3H_8O_2}} ZrO_2 + H_2O + CO_2 + N_2$

Stoichiometric amounts of zirconium nitrate and urea are calculated based upon propellant chemistry. The fuel to oxidizer ratios were calculated using the equation below [39], [58], [59]:

$$\phi = \frac{RV}{OV} n \Leftrightarrow n = 1 \times \frac{OV}{RV} \quad (4)$$

Where RV is the valency of the reducing reagent and OV is the valency of the oxidizing reagent; n is the number of moles of fuel per mole of oxidant and $\varphi = 1$ indicates that is not necessary any molecular oxygen for the reaction being complete and thus the optimal stoichiometric composition of redox mixture is obtained [38].

In order to calculate the oxidizing/reducing is necessary to define the valences of a redox mixture. The zirconium, carbon and hydrogen are considered as reducing elements (+4 for zirconium, +4 for carbon and +1 for hydrogen) and oxygen and nitrogen are seen as an oxidizer (-2 for oxygen and 0 for nitrogen) [39]. The RV and the OV calculated are shown in Table below.

Table 6.2 - Valence of the oxidizer and the reducer.

Reagents	Chemical Formula	Calculation	Total
Oxidizing reagent (OV)	$ZrO(NO_3)_2$*	4-2 + (2 × 0) + (3 × 2 × -2)	-10
Reducing reagent (RV)	$CO(NH_2)_2$	4-2 + (2 × 0) + (2 × 2 × 1)	+6

*Hydration water does not affect the overall compound valence

Substituting the *OV* and *RV* values in the equation (1), we obtain $n = 5/3$ (Table 6.3).

Table 6.3 - Number of moles (n) to ensure stoichiometry of the redox reaction.

Precursor	ϕ	Fuel	n
Zirconium oxide nonahydrate	1	Urea	$\left(\frac{5}{3}\right)$

The magnitudes of the total reducing and oxidizing valences serve as numerical coefficients for the oxidizer and the fuels for stoichiometric balance. The stoichiometrically balanced equation is presented in the Table 6.4.

Table 6.4 - Overall reaction given by the combination of reduction and oxidation reaction.

Precursor	Fuel	Overall Reaction
Zirconium oxide nonahydrate	Urea	$3ZrO(NO_3)_2(s) + 5CO(NH_2)_2(g) \xrightarrow{\mathbf{C_3H_8O_2;\ T_b = 124\ °C}} 3ZrO_2(s) + 10H_2O(g) + 5CO_2(g) + 8N_2(g)$

During combustion, the gaseous products released were N_2 CO_2, N_2 and H_2O as water vapor. We assume that the brown fumes observed during combustion were released in the form of the above gaseous products.

6.2. Annex B

Schematics of MIS and MIM capacitors fabrication steps, figure 6.1 and 6.2, respectively.

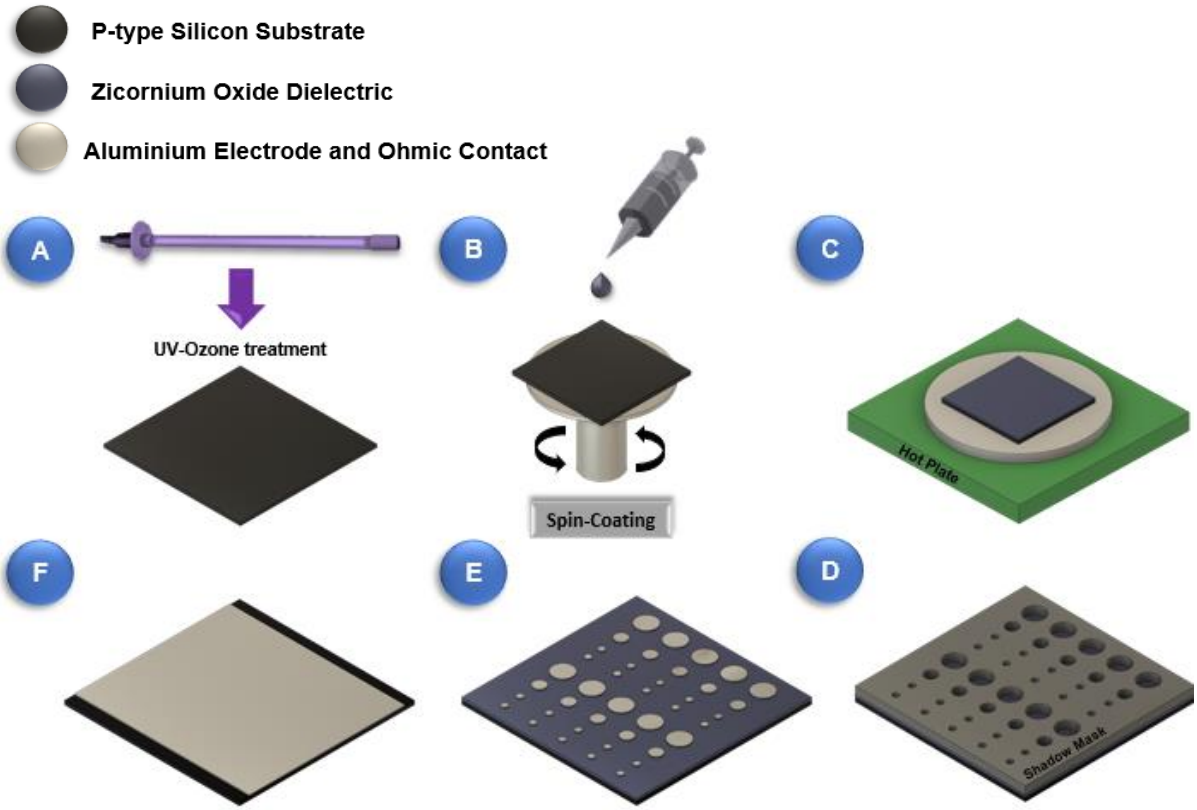

Figure 6.1 - MIS capacitor fabrication steps after the cleaning process: (A) Surface treatment on Si substrate by UV-ozone for 15 min; (B) Deposition of precursor solution by spin coating; (C) Substrate submitted an annealing temperature for film densification; (D) After placed the shadow Mask upon the dielectric film; (E) After top electrodes deposition (80 nm Al) by thermal evaporator; (F) After 80 nm Al layer deposition by thermal evaporation for optimize the ohmic contact.

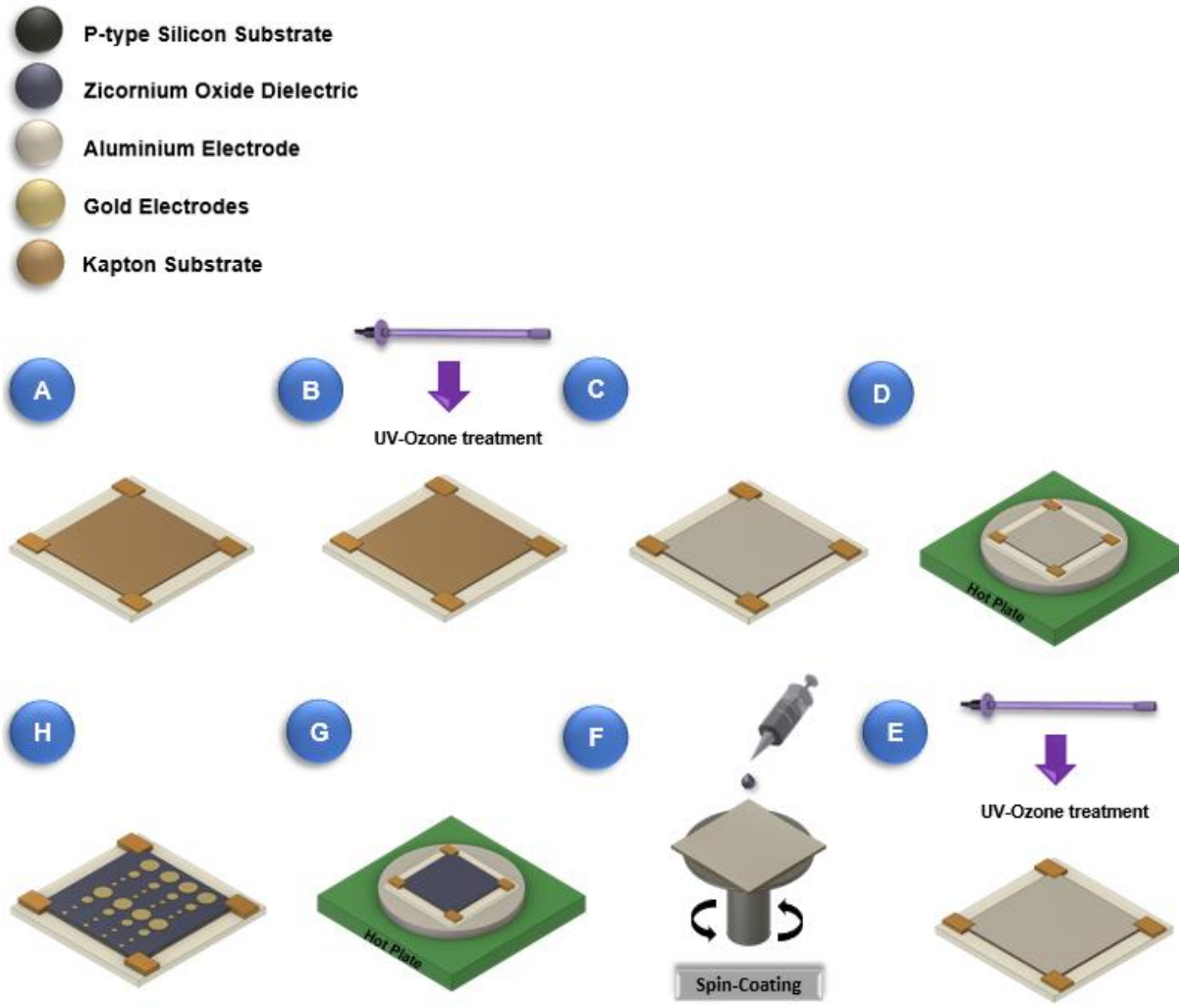

Figure 6.2 - MIM capacitor fabrication steps after the cleaning process: (A) After placed the Kapton (Flexible substrate) upon a 3x3 cm glass substrate; (B) Surface treatment by UV-ozone for 15 min ; (C) After electrode (80 nm Al) deposition upon Kapton; (D) Substrate submitted to a 180 °C thermal treatment for 10 min; (E) Surface treatment by UV-ozone for 15 min; (F) Deposition of precursor solution by spin coating; (G) Thin film submitted to thermal treatment; (H) After top electrodes (80 nm Au) deposition with a e-beam evaporator and a shadow mask.

6.3. Annex C

Surface images of ZrO_x thin films from optical microscope.

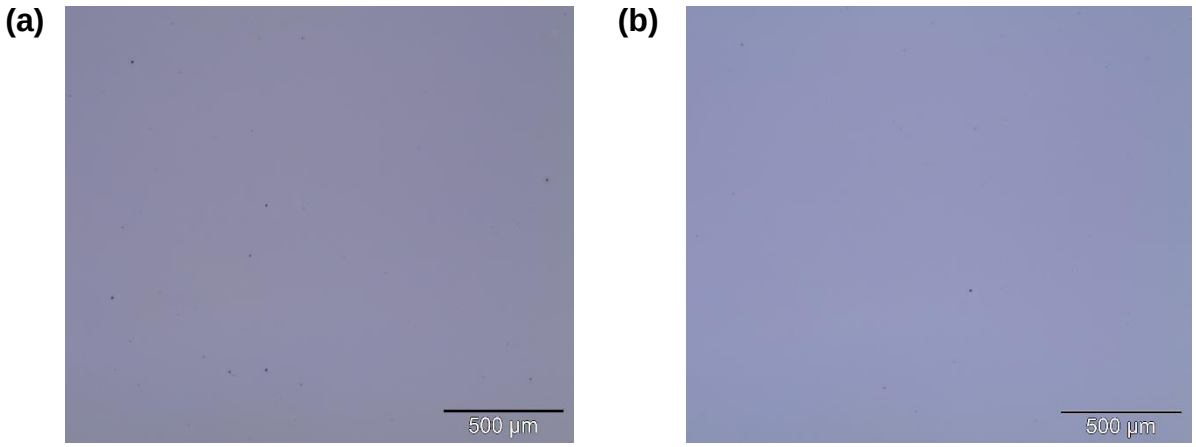

Figure 6.3 - Surface images from optical microscope for (a) ethanol and (b) 2-ME solution-based ZrO_x thin films deposited on silicon.

6.4. Annex D

Thickness and band gap values for different conditions and precursor concentrations for solution-based ZrO_x thin films depicted in Table 6.5.

Table 6.5 - Thickness and band gap with the respective relative errors of the ZrO_x thin films at different conditions, concentrations and solutions solvents ("-" means that the respective condition was not measured for this concentration).

Condition	Nº of layers	Solvent	c (M)	d_{high-K} (nm)	E_g (eV)
150 °C + DUV, 30 min	1	Ethanol	0.1	-	-
			0.2	25.7 ± 0.1	4.2 ± 0.1
		2-ME	0.1	-	-
			0.2	18.3 ± 0.1	5.1 ± 0.1
150 °C + DUV, 1 h	1	Ethanol	0.1	13.3 ± 0.1	5.1 ± 0.1
			0.2	24.0 ± 0.1	4.2 ± 0.1
		2-ME	0.1	9.6 ± 0.1	5.6± 0.1
			0.2	16.0 ± 0.1	5.3 ± 0.03
250 °C, 30 min	1	Ethanol	0.1	15.1 ± 0.1	5.1 ± 0.1
			0.2	24.8 ± 0.1	4.9 ± 0.02
		2-ME	0.1	10.8 ± 0.1	5.0 ± 0.1
			0.2	15.6 ± 0.05	5.1 ± 0.2
300 °C, 30 min	1	Ethanol	0.1	14.9 ± 0.1	5.3 ± 0.04
			0.2	21.9 ± 0.1	4.1 ± 0.04
		2-ME	0.1	9.9 ± 0.1	5.0 ± 0.1
			0.2	13.9 ± 0.2	5.1 ± 0.03
300 °C, 30 min	2	2-ME	0.2	33.8 ± 0.1	4.1 ± 0.1
350 °C, 30 min	1	Ethanol	0.1	13.4 ± 0.1	4.9 ± 0.1
			0.2	21.1 ± 0.1	4.5 ± 0.1
		2-ME	0.1	8.7 ± 0.1	5.2 ± 0.04
			0.2	14.2 ± 0.1	5.1 ± 0.1

6.5. Annex E

Characteristic parameters (Capacitance at 1 kHz, dielectric constant and Breakdown Electric Field) for 0.2 M ZrO_x films produced at different conditions (150 °C combined with DUV irradiation for 30 min and 1 h, 250 °C, 300 °C and 350 °C for 30 min) and with different solutions (Zirconium nitrate in ethanol anhydrous or zirconium nitrate with urea as fuel in 2-ME).

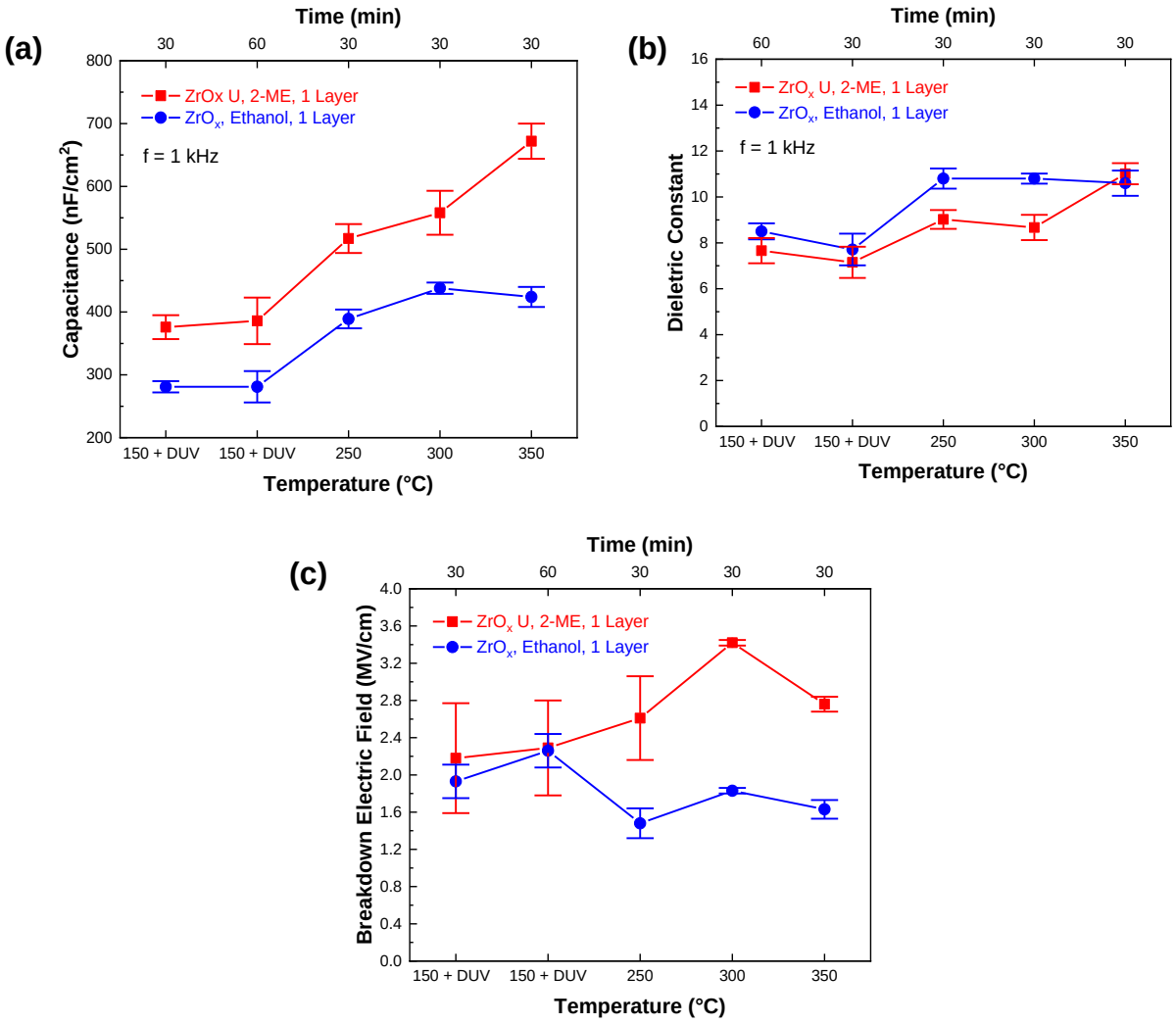

Figure 6.4 - Electrical properties of 2-ME and Ethanol solution-based capacitors: (a) Capacitance at 1 kHz, (b) dielectric constant and (c) breakdown electric field in function of temperature and time.

6.6. Annex F

Electrical characterization by $C-V$, $I-V$ and $C-f$ measurements of ZrO_x MIS capacitors with dielectric thin films deposited on Si for a zirconium nitrate concentration of 0.1 M in different solvents, Ethanol and 2-ME (Figure 6.5 and 6.6, respectively). Different annealing temperatures were applied to the films: 250 °C, 300 °C and 350 °C for 30 min

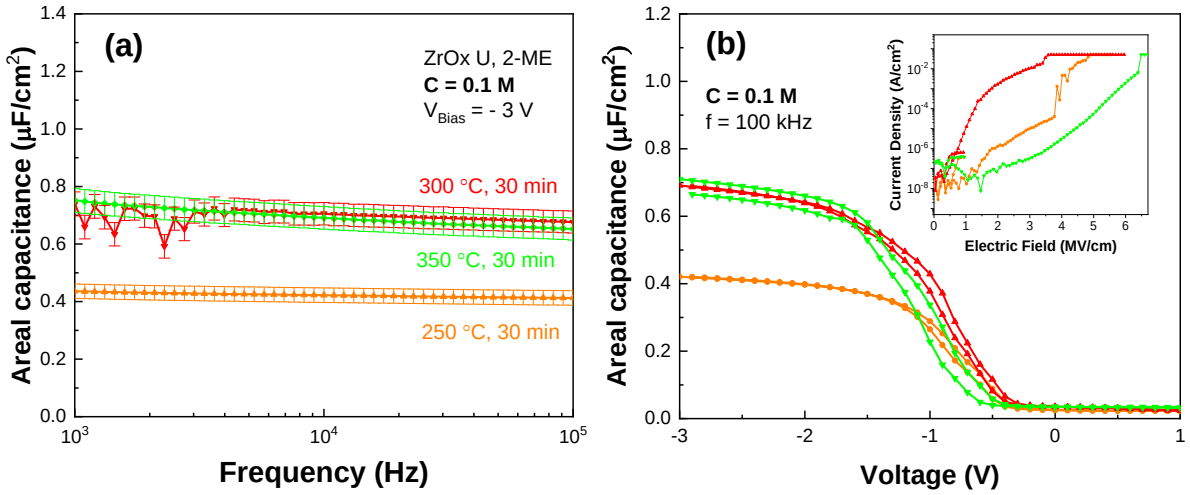

Figure 6.5 – Characteristic curves of 2-ME solution-based Al/ZrO_x/p-Si capacitors for a precursor concentration of 0.1 M at different annealing temperatures: (a) Areal capacitance-frequency, (b) areal capacitance-voltage and current density-electric field in the inset.

Table 6.6 - Summary of the physical and electrical properties of the devices depicted in the Figure 6.5 (0.1 M concentration) and the devices with 0.2 M presented in the sub-section 3.3.2.

Condition	**Solvent**	***c*** (M)	C_i (nF cm^{-2}) **at 1 kHz**	$d_{high-\kappa}$ (nm)	**κ at 1 kHz**	***E*** (MV cm^{-1})	***J*** (A cm^{-2}) **at 1 MV/m**
250 °C, 30 min	2-ME	0.1	436 ± 25	10.8 ± 0.1	5.3 ± 0.3	4.1 ± 0.2	(1.7 ± 3.5) × 10^{-8}
	2-ME	0.2	517 ± 23	15.7 ± 0.1	9.0 ± 0.4	2.6 ± 0.5	(2.1 ± 23.6) × 10^{-6}
300 °C, 30 min	2-ME	0.1	739 ± 32	9.9 ± 0.1	8.0 ± 0.4	3.7 ± 0.9	(8.5 ± 21.7) × 10^{-5}
	2-ME	0.2	558 ± 35	13.9 ± 0.2	8.7 ± 0.5	3.4 ± 0.03	(2.2 ± 2.7) × 10^{-8}
350 °, 30 min	2-ME	0.1	751 ± 41	8.7 ± 0.1	7.4 ± 0.4	6.0 ± 0.4	(5.6 ± 1.6) × 10^{-8}
	2-ME	0.2	672 ± 28	14.2 ± 0.1	11.0 ± 0.5	2.8 ± 0.1	(3.9 ± 1.1) × 10^{-7}

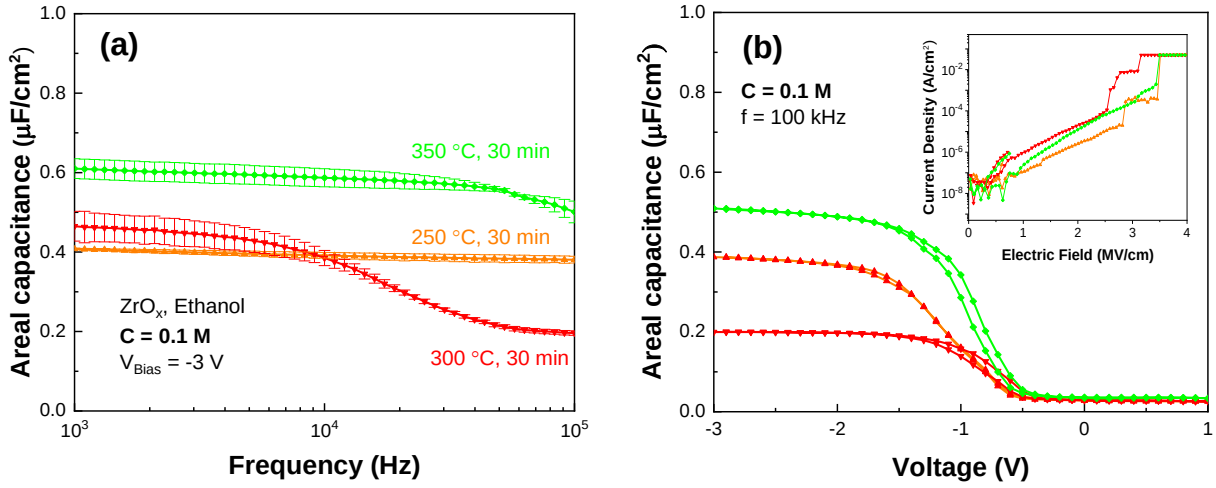

Figure 6.6 - Characteristic curves of ethanol solution-based Al/ZrO_x/p-Si capacitors for a precursor concentration of 0.1 M at different annealing temperatures: (a) Areal capacitance-frequency, (b) areal capacitance-voltage and current density-electric field in the inset.

Table 6.7 - Summary of the physical and electrical properties of the devices depicted in the Figure 6.6 (0.1 M concentration) and the devices with 0.2 M presented in the sub-section 3.3.2.

Condition	**Solvent**	***c*** (M)	C_i (nF cm^{-2}) **at 1 kHz**	$d_{high-\kappa}$ (nm)	**κ at 1 kHz**	***E*** (MV cm^{-1})	***J*** (A cm^{-2}) **at 1 MV/m**
250 °C, 30 min	Ethanol	0.1	408 ± 11	15.1 ± 0.1	6.9 ± 0.2	3.3 ± 0.5	(1.2 ± 0.7) × 10^{-7}
	Ethanol	0.2	389 ± 15	24.8 ± 0.1	10.8 ± 0.4	1.5 ± 0.2	(2.3 ± 29.9) × 10^{-6}
300 °C, 30 min	Ethanol	0.1	465± 56	14.0 ± 0.1	7.4 ± 0.9	3.1 ± 0.7	(1.1 ± 15.8) × 10^{-6}
	Ethanol	0.2	438 ± 9	21.9 ± 0.1	10.8 ± 0.2	1.8 ± 0.03	(8.7 ± 0.4) × 10^{-7}
350 °C, 30 min	Ethanol	0.1	610 ± 24	13.4 ± 0.1	9.4 ± 0.4	2.7 ± 0.2	(2.6 ± 3.2) × 10^{-7}
	Ethanol	0.2	424 ± 16	21.0 ± 0.1	10.6 ± 0.5	1.6 ± 0.1	(4.3 ± 2.7) × 10^{-8}

6.7. Annex G

With the atomic force microscopy (AFM) was possible to obtain the roughness of the outside and inside surface of a 75 µm Kapton. The Figure 6.7 demonstrate that dielectric films should be deposited on the outside surface of the Kapton due to the lower roughness exhibited by this.

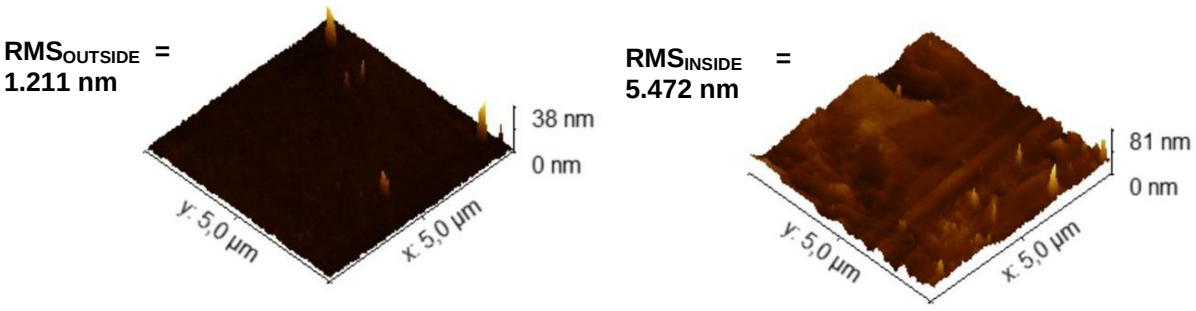

Figure 6.7 – AFM substrate analysis: The left image shows the outside surface of the kapton which exhibits a roughness of 1.211 nm. The right image shows the inside surface of it with a roughness of 5.472 nm.

The surface roughness also depends on the annealing temperature. The Figure 6.8 shows that the 150 °C treatment for 1 h increases surface roughness by almost 3 times.

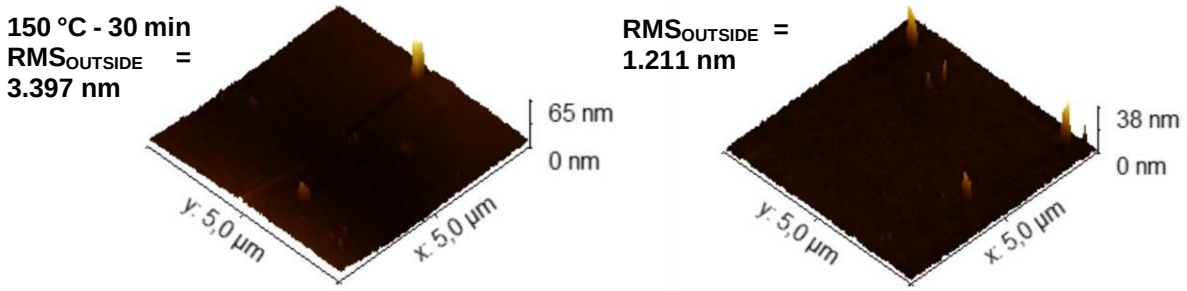

Figure 6.8 – AFM substrate analysis: The left image shows the surface of the kapton after the annealing process at 150 for 1 h which exhibits a roughness of 3.397 nm . The right image shows the outside surface without annealing with a roughness of 1.211 nm.

6.8. Annex H

Electrical characterization of ZrO_x MIS devices produced from $ZrO(NO_3)_2$ precursor solution using 2-ME as solvent and urea (U) as fuel (Figure 6.9) by capacitance-voltage (CV), capacitance-frequency (Cf) and current-voltage (IV) curves. The dielectric film was treated combining FUV irradiation and thermal annealing at 200 °C for 30 min. The electrical properties of the MIS device are shown in the

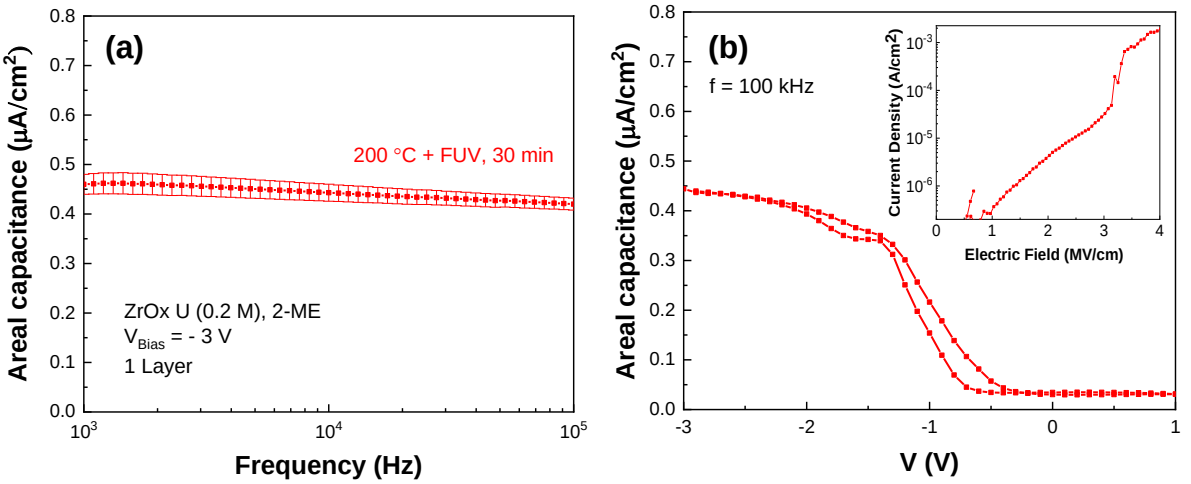

Figure 6.9 - Characteristic curves of 2-ME solution-based Al/ZrO_x/p-Si capacitors annealed at 200 °C combined with FUV irradiation for 30 min: a) areal capacitance-frequency and b) areal capacitance−voltage to a frequency of 100 kHz with current density-electric field in the inset.

Table 6.8 - Electrical properties obtained for the devices depicted in Figure 6.9.

Condition	**Solvent**	***c*** (M)	C_i (nF cm^{-2}) **at 1 kHz**	$d_{high-\kappa}$ (nm)	**κ at 1 kHz**	***E*** (MV cm^{-1})	***J*** (A cm^{-2}) **at 1 MV cm^{-1}**
200 °C + FUV, 30 min	2-ME	0.2	460 ± 20	15 ± 0.1	7.8 ± 0.3	3.2 ± 0.5	(3.7 ± 14.6) × 10^{-7}

6.9. Annex I

Comparative of our results with literature in the Table 6.9.

Table 6.9 - Selected processing details for several reported solution-based ZrO_x deposited by spin-coating ("-" means that the related data is not mentioned in the literature).

Year	Solvent	c (M)	Substrate/ Structure	Annealing Temperature (°C)	t_A (min)	C_i (nF cm^{-2}) at 1 kHz	$d_{high-\kappa}$ (nm)	κ at 1 kHz	E (MV cm^{-1})	J (A cm^{-2}) at 1 MV cm^{-1}
2013 [15]	2-ME	0.3	glass / MIM	300	-	~155	120	21	-	-
2014 [29]	DMF	0.1	Si / MIS	UV assisted	30	~750	5.5	~9.5	9.5	~1.0×10^{-9}
2015 [3]	DMF	0.1	Si / MIS	150	33	~302	14.6	~6.2	7.7	~7.0×10^{-9}
2016 [5]	2-ME	0.2	Si / MIS	350	120	138	139	21.7	-	-
			Si / MIS	250	120	97	143	15.7	-	-
2017 [30]	Ethanol	0.2	Si / MIS	UV assisted	80	~750	-	~12	-	-
2017 [2]	2-ME	0.3	glass / MIM	400	-	300	66.9	15-22	-	-
		0.1	glass / MIM	400	-	760	22.5	15-22	-	-
2018 [18]	2-ME	0.1	Si / MIS	400	60	313	18.8	5.7	-	~9.0×10^{-10}
		0.1	Si / MIS	300	60	388	18.3	7.1	-	~9.0×10^{-10}
2018 [6]	2-ME	-	glass / MIM	300	60	-	150	~10.5	> 4.0	5.0×10^{-8}
2018 [1]	DMF	0.15	Si / MIS	300	60	219	40.3	8.8	-	-
			Si / MIS	160	60	117	59	7.8	-	-
This study	2-ME	0.2	Si / MIS	300	30	558	13.9	8.7	3.4	2.2×10^{-7}
	Ethanol	0.2	Si / MIS	300	30	438	21.9	10.8	1.8	8.7×10^{-7}
	2-ME	0.1	Si / MIS	350	30	751	8.7	7.4	6.0	2.7×10^{-8}
	Ethanol	0.1	Si / MIS	350	30	610	13.4	9.4	2.7	2.6×10^{-7}
	2-ME	0.2	Si / MIS	150 + DUV assisted	60	386	16	7.1	2.3	1.4×10^{-6}
	2-ME	0.2	Kapton / MIM	150 + DUV assisted	60	302	33.8	11	1.0	1.2×10^{-4}